NOTICE

The quality of this microform is heavily dependent upon the quality of the original thesis submitted for microfilming. Every effort has been made to ensure the highest quality of reproduction possible.

If pages are missing, contact the university which granted the degree.

Some pages may have indistinct print especially if the original pages were typed with a poor typewriter ribbon or if the university sent us an inferior photocopy.

Reproduction in full or in part of this microform is governed by the Canadian Copyright Act, R.S.C. 1970, c. C-30, and subsequent amendments.

AVIS

La qualité de cette microforme dépend grandement de la qualité de la thèse soumise au microfilmage. Nous avons tout fait pour assurer une qualité supérieure de reproduction.

S'il manque des pages, veuillez communiquer avec l'université qui a conféré le grade.

La qualité d'impression de certaines pages peut laisser à désirer, surtout si les pages originales ont été dactylographiées à l'aide d'un ruban usé ou si l'université nous a fait parvenir une photocopie de qualité inférieure.

La reproduction, même partielle, de cette microforme est soumise à la Loi canadienne sur le droit d'auteur, SRC 1970, c. C-30, et ses amendements subséquents.

ISBN 0-315-56102-5

Canada

Characterization of Electrochemical Photovoltaic Cells Using Polycrystalline CdSe and CdTe Grown by Liquid Metal-Vapour Reaction

Zhitsing Deng

A Thesis

in

The Department

of

Chemistry

Presented in Partial Fulfillment of the Requirements
for the Degree of Master of Science at
Concordia University
Montréal, Québec, Canada

April 1990

ABSTRACT

Characterization of Electrochemical Photovoltaic Cells Using Polycrystalline CdSe and CdTe Grown by Liquid Metal-Vapour Reaction

Zhitsing Deng

Polycrystalline cadmium selenide and cadmium telluride layers were fabricated by putting liquid cadmium metal in contact with argon / selenium or tellurium vapour atmosphere. The results presented in this thesis show that, under the proper experimental conditions, the liquid metal-vapour reaction enables the synthesis of polycrystalline CdSe semiconductor layers which have a 6.9% conversion efficiency when in contact with a 1M polysulfide electrolyte under white light illumination. This value rates amongst the highest efficiencies measured under similar conditions with polycrystalline CdSe in a electrochemical photovoltaic cell.

The physical structure of these electrodes has been studied by scanning electron microscopy, x-ray diffraction, energy dispersive x-ray analyses. The highly textured surface of the samples seem to be responsible for the high photovoltaic efficiency.

In this process, no post-etch or post-annealing treatment is needed. The semiconductor is grown directly on the metal plate, It therefore provides a good ohmic contact and is relatively stable when in contact with polysulfide electrolyte.

ACKNOWLEDGEMENTS

I wish to express my appreciation to my supervisor, Dr. M. Lawrence for his guidance.

I would like to thank the members of my research committee, Dr. N. Serpone and Dr. P. H. Bird, for their cooperation and helpful suggestions.

I am deeply indebted to Mr. Z. Huang and other colleagues, for their invaluable aid.

I would like to give special thanks to my wife, for her love and support.

To my wife: Xu

CONTENTS

LIST OF FIGURES

LIST OF TABLES

CHAPTER 1

INTRODUCTION

1.1 Solar Cells

Solar cells at present furnish the most important long-duration power supply for satellites and space vehicles. Solar cells have also been successfully employed in small-scale terrestrial applications. As worldwide energy demand increases, conventional energy resources, such as fossil fuels, will be exhausted in the not-too-distant future. Therefore, we must develop and use alternative energy resources, especially our only long-term natural resource, the sun. The solar cell is considered a major candidate for obtaining energy from the sun, since it can convert sunlight directly to electricity with high conversion efficiency, can provide nearly permanent power at low operating cost, and is virtually free of pollution.

The solar cell was first developed by Chapin, Fuller, and Pearson in 1954 using a diffused silicon *p-n* junction[1]. Then Brattain described the behaviour of germanium when it was polarized in aqueous electrolytes[2,3]. To date, solar cells have been made with many other semiconductors, using various device configurations and employing single-crystal, polycrystalline, and amorphous thin-film structures.

1.2 Electrochemical Photovoltaic Cells

Photoelectrochemistry is based principally on the semiconductor electrode. It is the semiconductor's ability to absorb light and covert it to electrical and / or chemical energy that forms the basis for the semiconductor liquid junction solar cell.

In the case where optical energy is converted into electrical energy, the cells are called electrochemical photovoltaic cells.

Photoelectrochemistry has forced the alliance of solid state physics with electrochemistry. Out of this alliance has arisen a common terminology and a convention for representing the semiconductor electrode / electrolyte interface. The convention is largely based on the energy band theory of solid state physics.

1.3 Semiconductors

How does a semiconductor work in producing a solar cell?

A perfect semiconductor crystal with no impurities or lattice defects is called an intrinsic semiconductor. Figure 1.1 is an intrinsic semiconductor energy level diagram. The lowest empty band is called the conduction band (Ec), and the highest filled band the valence band (Ev) which contains many electrons. The valence band is derived from the bonding molecular orbitals of the crystal, and the conduction band from the antibonding orbitals. The gap where no available energy levels appear in between the valence band and conduction band is called the bandgap (Eg). At 0^0K, an intrinsic semiconductor is a non-conductor, because its valence band is completely occupied and its conduction band totally empty. Mobile charge carriers, however, can be generated by different mechanisms, such as thermal excitation, and photo-excitation.

When impurities which act as dopants are purposely introduced in intrinsic semiconductors, the resulting material is referred to as an extrinsic semiconductor. The extrinsic semiconductors in which the electrical current is carried predominantly

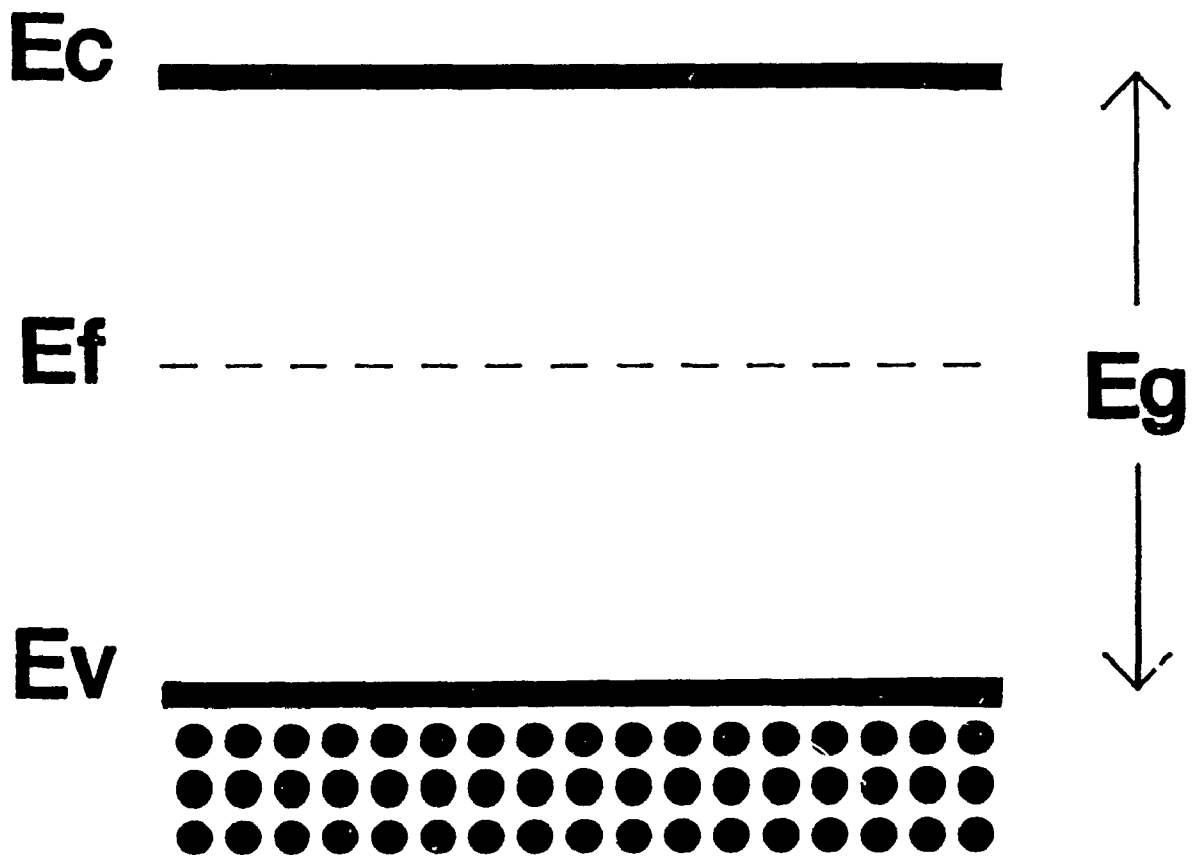

Figure 1.1 The intrinsic semiconductor energy level diagram. Ec = Conduction band energy level; Ev = Valence band energy level; Eg = Bandgap energy; Ef = Fermi level.

by negatively charged carriers, that is by excess electrons in the conduction band due to the presence of appropriate donor impurities, with energies a few kT below the conduction band, are called *n*-type (Figure 1.2). The corresponding *p*-type semiconductor is created when electron acceptors have energy levels with a few kT above the valence band edge. Electrons are captured from the valence band, creating an excess population of positive charge carriers, holes, in the valence band.

Electrons can be promoted from the valence band to the conduction band upon the absorption of light. A necessary condition for absorption is that the incident photon energy equals or exceeds the bandgap energy ($h\nu \geq E_g$). A photon with energy greater than E_g contributes an energy E_g to the cell's electrical output, and the energy in excess of E_g is converted into heat. This is the primary event in the conversion of sunlight to usable forms of energy.

1.4 Fermi Level

The Fermi level (E_f) corresponds to the energy (E) at which the probability of occupation by electrons is exactly half. It represents an important quantity in the analysis of semiconductor behaviour. The probability of occupancy increases with energies below the Fermi level and decreases with energies above the Fermi level in accordance with the Fermi-Dirac distribution function:

$$f(E) = \frac{1}{1 + \exp \dfrac{E - E_f}{kT}} \qquad (1.1)$$

where k is the Boltzmann's constant (1.38×10^{-23} JK^{-1}). T is the absolute

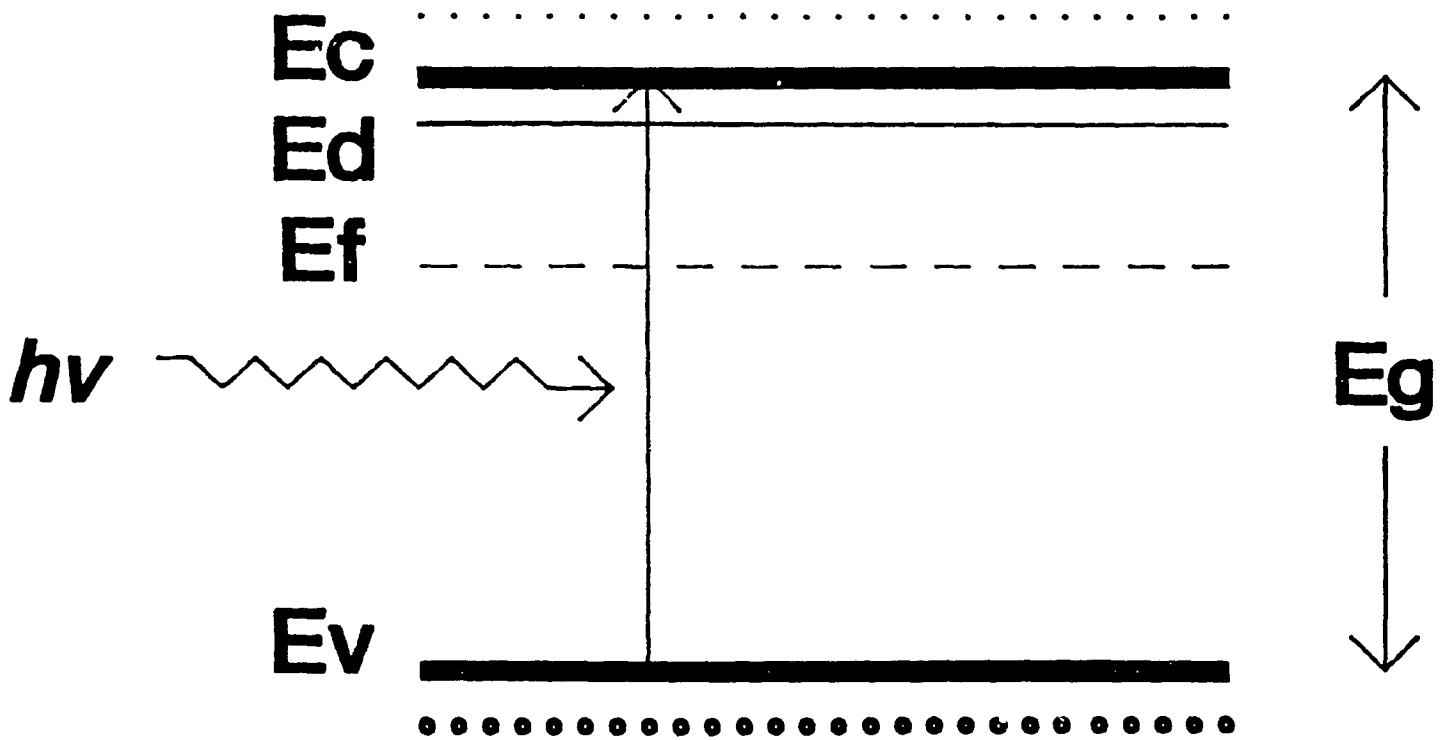

Figure 1.2 The n-type semiconductor energy level diagram. Ed = Donor energy level.

temperature.

For intrinsic materials, the concentration of holes in the valence band is equal to the concentration of electrons in the conduction band. Therefore, the Fermi level must lie at the middle of the bandgap (Figure 1.1). In *n*-type materials there is a high concentration of electrons in the conduction band compared with the hole concentration in the valence band. Thus in *n*-type materials the Fermi level must lie above its intrinsic position on the energy scale (Figure 1.2). A similar but opposite effect is observed in *p*-type materials.

1.5 Semiconductor Electrode - Electrolyte Junction

When *n*-type and *p*-type semiconductors are put in contact, the electrons, which are abundant on the "n" side, diffuse into the "p" side. Holes diffuse in the opposite direction. These cause an immediate loss of neutrality: the "n" side, loosing electrons, becomes positive because of the net donor charge left behind; the "p" side similarly becomes negatively charged. As the diffusion proceeds, the potential barrier builds up across the junction to reach a value at which any further majority carrier diffusion is blocked. At this point, the system is at equilibrium and the Fermi levels are equal in both materials. A region is therefore created on both sides of the *p-n* junction, in which there is a built-in field and in which there is a depletion of mobile charge carriers. This region is called the depletion layer. A depletion layer is generally developed by a semiconductor electrode upon contact and equilibration of the Fermi level with a second phase.

All phenomena associated with photoelectrochemical systems are based on the formation of a semiconductor electrode - electrolyte junction when an appropriate semiconductor electrode is immersed in an appropriate electrolyte. Application of the equilibration concept to the semiconductor electrode / electrolyte interface requires the definition of the Fermi level in an electrolyte. For liquid electrolytes, the Fermi level is determined by the redox potential of the redox couples present in solution and is identified with the Nernst potential according to following equations:

$$OX + ne^- = RED \qquad (1.2)$$

$$V_{rdx} = V^0 - \frac{RT}{nF} \ln \frac{[RED]}{[OX]} \qquad (1.3)$$

$$E_{rdx} = q\, V_{rdx} \qquad (1.4)$$

where OX is the oxidized form and RED the reduced form of the redox couple; n is the number of electrons transferred per molecule and q is the electron charge. Equation 1.3 is the Nernst expression, where V_{rdx} and V^0 are the Nernst potential and standard potential respectively. E_{rdx} corresponds to the "Fermi level" of the electrolyte solution expressed on the absolute energy scale, whose reference point is defined below. The solution "Fermi level" arises from the concept that OX and RED molecules in an electrolyte form a set of electron energy levels, of which the OX molecules are the unoccupied levels and the RED molecules are the occupied ones. When a semiconductor electrode is immersed in an electrolyte containing a redox couple, the Fermi level of the semiconductor electrode shifts with charge flow across the interface until $E_f = E_{rdx}$.

The semiconductor electrode Fermi level corresponds directly with the potential scale (Figure 1.3). By convention, the Fermi level is defined relative to the energy of an electron in vacuum (absolute energy scale), while the electrochemical potential scale is defined relative to the standard hydrogen electrode. The two scales are related by the theoretical value for the Fermi level of the SHE:

$$V = \frac{-4.5\ (eV) - E}{q} \qquad (1.5)$$

The electrochemical potential scale increases as the absolute energy scale decreases; electrons spontaneously flow from more negative to more positive potentials.

If the initial Fermi level in an *n*-type semiconductor is above the initial Fermi level in the electrolyte, then equilibration of the two Fermi levels occurs by transfer of electrons from the semiconductor to the electrolyte. This produces a positive space charge layer in the semiconductor which is also called a depletion layer since the region is depleted of majority charge carriers. The term "space charge" refers to the presence of a charge occupying the volume near the surface, the charge results from the charged doping sites or the accumulation of holes or electrons at the surface. As a result, the conduction and valence band edges are bent such that a potential barrier is established against further electron transfer into the electrolyte (Figure 1.4). The electric field thus created at the interface enables spatial separation of photogenerated electron-hole pairs, therefore, producing electric current.

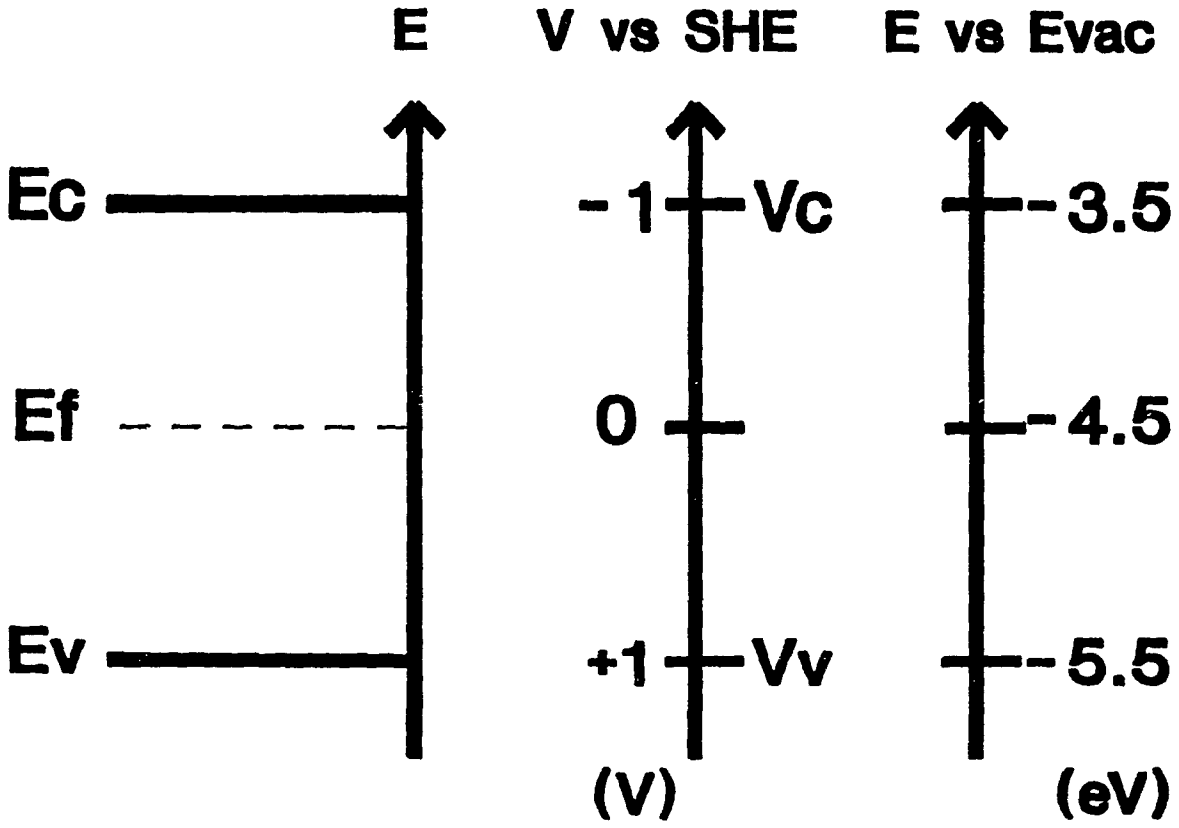

Figure 1.3 The absolute energy and electrochemical potential scales for a intrinsic semiconductor with E_g = 2.0 eV.

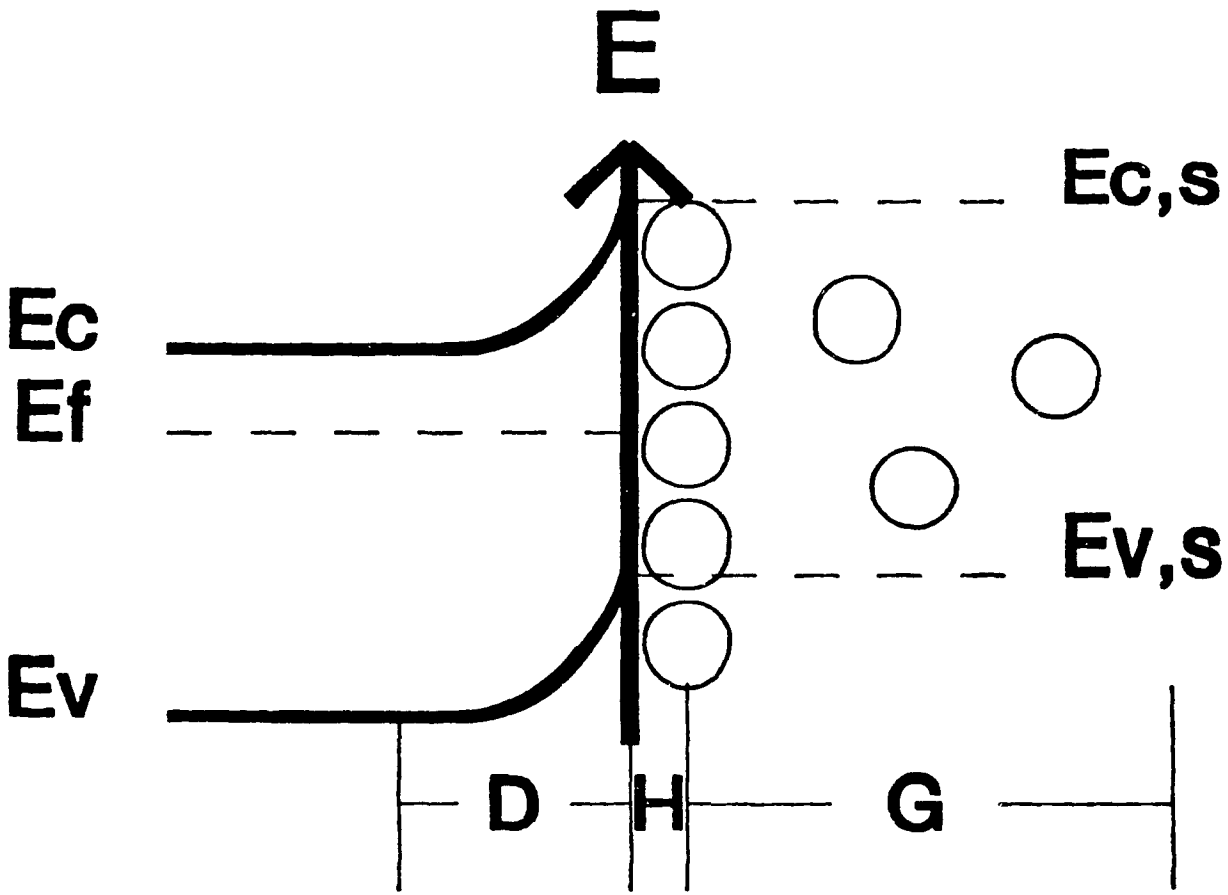

Figure 1.4 Energy level diagram for n-type semiconductor-electrolyte junction H = Helmholtz layer; G = Gouy layer; D = Depletion layer; Ec,s = Conduction band energy level of the surface; Ev,s = Valence band energy level of the surface.

1.6 The Effect of Applied Potential

In the electrochemical cell, all changes in the potential applied to the semiconductor working electrode affect the potential drop across the semiconductor / electrolyte interface. At a fixed applied potential there are three regions of varying electrical po tial (Figure 1.4).[4] On the electrolyte side there are the Gouy layer (diffuse layer) and the Helmholtz layer. The Gouy layer is the thickness of electrolyte where the ion concentrations deviate from the bulk electrolyte values. The Helmholtz layer is the region between the electrode surface and the plane of closest approach for ions. Within the *n*-type semiconductor electrode there is a depletion layer, in which the electrical potential varies from the surface to the bulk value. The potential changes smoothly across the width of the depletion layer. Because an electron at a band edge exhibits different energies in regions of varying electrical potential, the band edges bend accordingly. The band-bending can be positive (upwards), with E_c and E_v higher at the surface than in the bulk (*n*-type semiconductor), or the band-bending can be negative (downwards, *p*-type semiconductor). The magnitude of the band-bending is equal to the total potential drop across the depletion layer, $E_{c,s} - E_{c,b}$, where s and b subscripts refer to the surface and the bulk. The Fermi level stays at constant energy from the bulk to the surface, so the position of the Fermi level relative to the band edges changes at the surface. An important consequence of this is that the hole and electron concentrations are perturbed at the surface relative to the bulk. This is described by the following expressions:

$$[n] = N_c \exp\left[- \frac{E_c - E_f}{kT} \right] \qquad (1.6)$$

$$[p] = N_v \exp\left[- \frac{E_f - E_v}{kT} \right] \qquad (1.7)$$

Where [n] and [p] are the electron and hole densities respectively, N_c and N_v are the "effective" density of energy levels at the conduction band edge and valence band edge.

Equations 1.6 and 1.7 predict that one type of charge carrier will be depleted and the other type enriched at the surface. For the case of positive band-bending shown in Figure 1.4, electrons are depleted and holes enriched. A more picturesque way of describing this is to state that electrons roll down the conduction band edge to the lower energy, and holes, like bubbles, rise to the higher position of the valence band edge.

1.7 The Effect of Illumination

For both photocurrent and photopotential generation, the semiconductor exhibits a threshold response to photon energy dictated by the bandgap energy. As an initial approximation photo-effects switch on as the wavelength of incident light decreases below λ_g (above E_g), the electrode is relatively sensitive to light. The wavelength for the onset of photo-effects is, therefore, given as:

$$\text{Wavelength } \lambda_g \text{ (nm)} = \frac{1240}{E_g \text{ (eV)}} \qquad (1.8)$$

The dependence of photocurrent or photopotential on excitation wavelength provides information about the bandgap energy and the nature of the optical transition (direct or indirect). In a direct bandgap semiconductor, a photon with an energy just equal

to the direct bandgap energy is absorbed with the creation of a hole and an electron. In the case of indirect absorption, the transition of the electron is followed by the emission of a phonon (quantized lattice vibration) of energy q.

$$E_g = h\nu - q \qquad (1.9)$$

So, in an indirect bandgap semiconductor, the transition of an electron from the valence band to the conduction band requires less energy. The equivalent absorption process generates a hole, an electron, and a phonon.

When an *n*-type semiconductor electrode is biased sufficiently positive of the flat band potential V_{fb} (the potential at which the bands are flat, that is no band-bending), the dark current are very low, due to the blocking effect of the depletion layer. Upon irradiation of the semiconductor through the electrolyte with light ($\lambda < \lambda_g$), large anodic photocurrents appear. These photocurrents arise from the flux of holes (minority carriers) arriving at the semiconductor / electrolyte interface.

After light absorption generates an electron-hole pair in the depletion layer, the electric field in the depletion layer separates the two charge carriers, with the electron moving toward the bulk of the crystal and the hole migrating toward the surface (Figure 1.5). The holes have an oxidizing power, and are capable of oxidizing a reduced (RED) molecule in solution. The electron in the conduction band flows via an external circuit to another electrode, the counter electrode where reduction takes place. In the electrochemical photovoltaic cell, the two electrode reactions are inverse to each other:

$$RED + h^+ = OX \qquad \text{(anode reaction)} \qquad (1.10)$$

$$OX + e^- = RED \qquad \text{(cathode reaction)} \qquad (1.11)$$

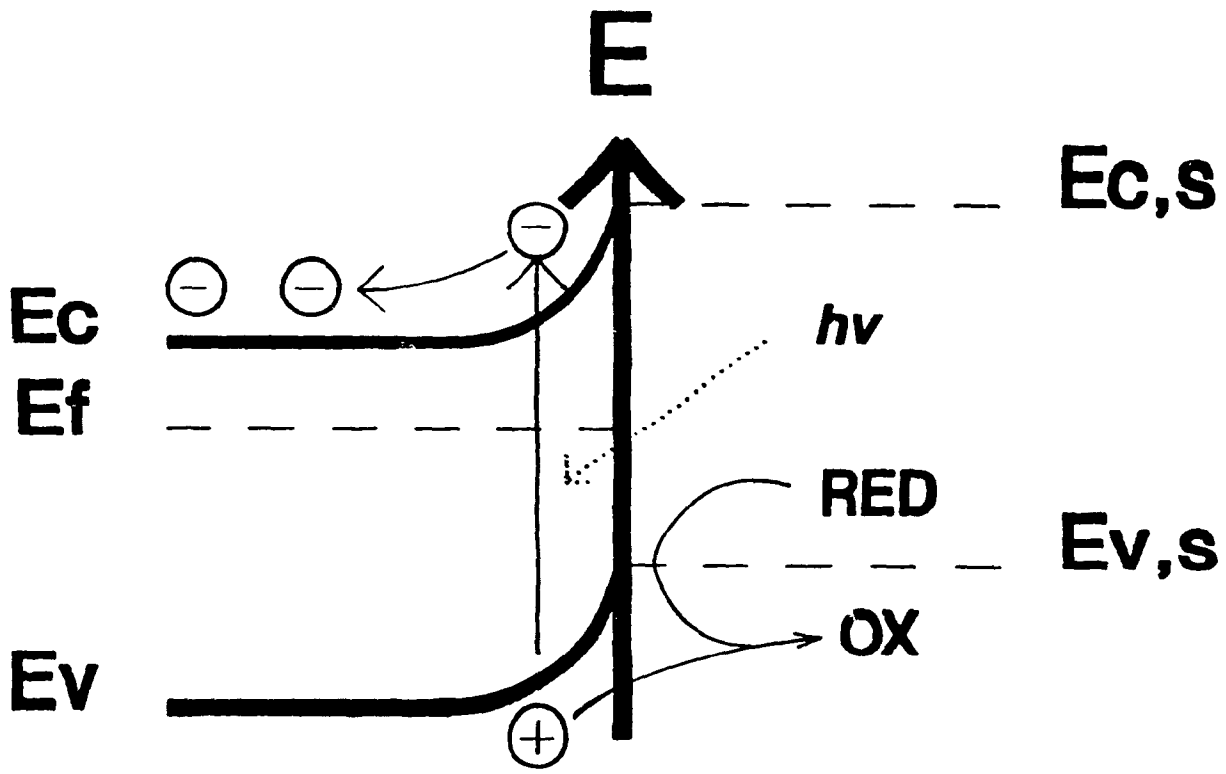

Figure 1.5 Photocurrent generation at a n-type semiconductor. Photogenerated holes move to the surface and oxidize reductants in the solution.

No net chemical change occurs in the electrolyte. The incident optical energy increases the energy of electrons in the semiconductor electrode, and electrical work is performed when these electrons traverse the external circuit to maintain the two electrode reactions.

The photocurrent versus applied voltage behaviour depends on the energy distribution of the incident photons, the absorption coefficient of the semiconductor, the diffusion length of the excited hole and electron, and the recombination rates. The simplest situation arises when the incident photons are absorbed within the depletion layer. Then the excited charge carriers are separated with minimum recombination. In the absence of mass transfer limitations imposed by the supply of hole acceptors (RED molecules), photocurrent quantum efficiencies (electrons collected per photon absorbed) approach unity. As long as the depletion layer thickness exceeds the depth of charge carrier generation, then photocurrent quantum efficiencies are independent of the applied potential.

As the applied potential approaches the flat band potential V_{fb}, the depletion layer thickness decreases. Recombination rates increase because the holes and electrons are no longer being separated by the electric field. The photocurrent drops sharply and merges with the dark current at V_{fb}. At potentials negative of V_{fb} the electrode is no longer blocking, so the dark current becomes cathodic and increases dramatically.

1.8 II-VI Semiconductors

The cadmium chalcogenides, CdX (X = S, Se, Te) are some of the most important semiconductors in photoelectrochemical research.

Table 1.1 shows the bandgap energy of these materials. The cadmium chalcogenides' maximum theoretical conversion efficiencies under direct sunlight are shown in Figure 1.6.[5]

Interest in regenerative electrochemical photovoltaic cells for solar energy conversion has resulted in a large body of literature on the preparation and characterization of economical CdX polycrystalline electrodes.[6,7] Because CdSe and CdTe have appropriate bandgaps for solar energy conversion (Figure 1.6), these compounds have been the focus of much research. Polycrystalline photoanodes, particularly of CdSe, have performed in some cases nearly as well as single crystals, underscoring the potential advantages of the intimate solid-liquid junction compared to solid-solid junctions. For more practical purposes, however, the main objective has remained the synthesis of CdTe, the II-VI semiconductor best adapted to solar energy conversion.

The forgiving nature of the semiconductor electrode / electrolyte interface has resulted in many different fabrication techniques being tried for electrochemical photovoltaic cells, including those which produce materials that are of much lower quality than would be required for a solid state device. Photoelectrodes with acceptable performance, sometimes approaching that of single crystals, have been produced by such techniques as vacuum evaporation,[8] electroplating,[9] screen printing, chemical bath deposition, spray pyrolysis, and pressure sintering.[10] To this list of

Semiconductor	Bandgap Energy E_g (eV)	Wavelength λ_g (nm)
CdS	2.4	520
CdSe	1.7	730
CdTe	1.4	890

Table 1.1 Cadmium chalcogenide semiconductors bandgap energy.

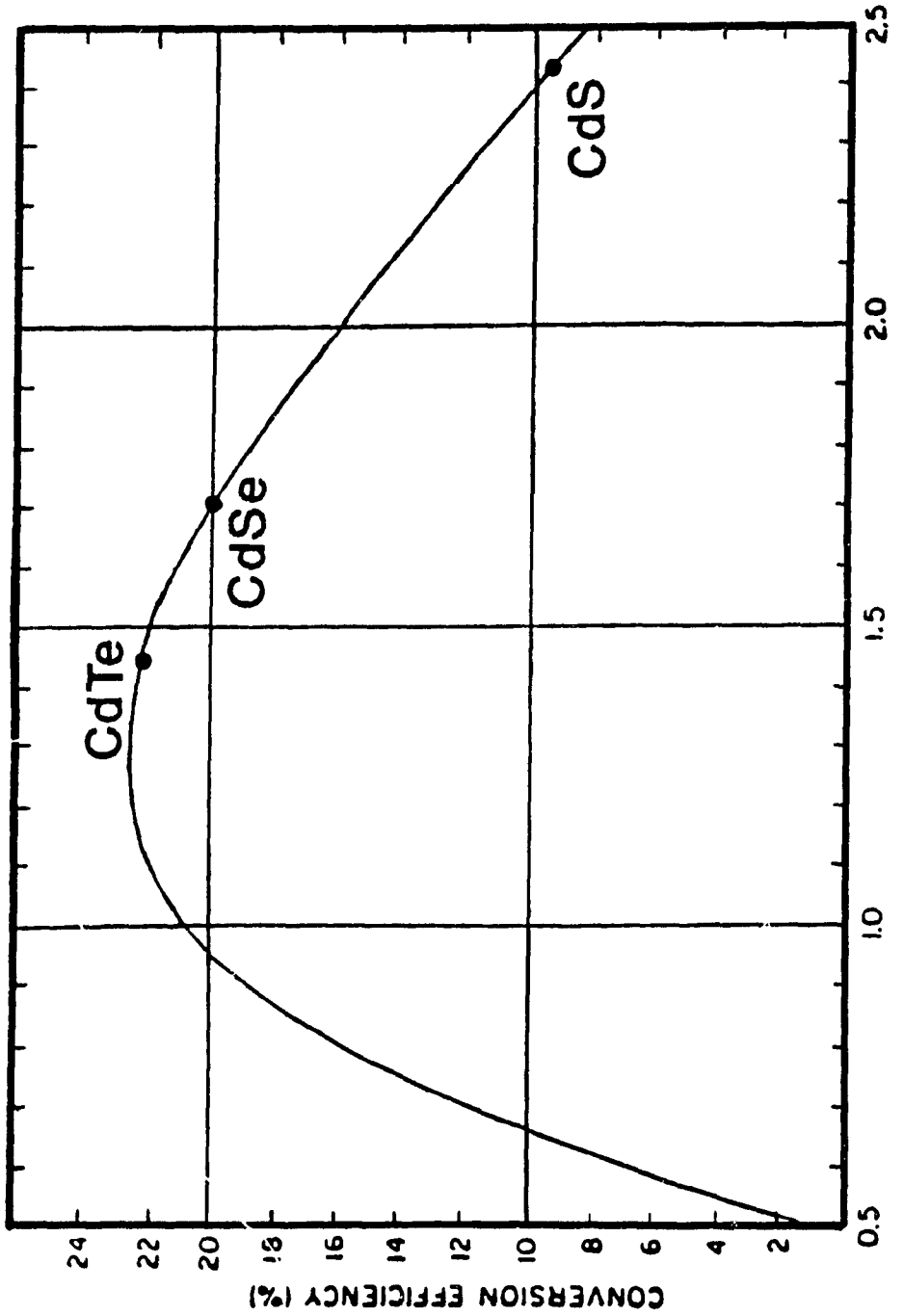

Figure 1.6 Maximum conversion efficiency of cadmium chalcogenides

cost-effective methods, a new method, the liquid metal-vapour process is presented in this thesis. This particular technique is an extension of the studies by Iwanov and Nanev concerning the direct synthesis of epitaxial II-VI semiconductor thin films on single crystal metal substrates,[11] have led to the development of another promising technique for the low-cost production of polycrystalline II-VI layer. This method, referred to in the past as the "tarnishing reaction"[12] or as the "gas-solid process",[13] involves the reaction of the chalcogen vapour with the surface of the heated metal substrate, under constant argon flow. It has been demonstrated that the gas-solid process, in its early stage of development, enables the synthesis of polycrystalline films of CdS, CdSe, ZnS and ZnSe on a variety of substrates. The substrate can either be a plate of the metal itself or be composed of the metal, deposited for example by evaporation, on a conductive glass plate (indium-tin-oxide coated glass) or on another metal (titanium).

Through these preliminary studies, the metal substrates used in the synthesis of the polycrystalline II-VI compounds were always maintained at temperatures below their melting points. For CdS and CdSe, the Cd substrates were kept at about 300°C (melting point of Cd is 321°C); for ZnS and ZnSe, the Zn substrates were kept at about 400°C (melting point of Zn is 420°C). At these temperatures, the reactions proceed as the chalcogen (X) vapours are brought in contact with the substrates' solid metal (M) surfaces under constant argon flow according to:

$$M_{(solid)} + X_{(vapour)} \xrightarrow[\text{Ar flow}]{\Delta} MX_{(solid)} \qquad (1.12)$$

The thickness of the semiconductor layer thus obtained varies with reaction time. Of the II-VI materials produced under these experimental conditions, CdSe gave the highest photovoltaic energy conversion efficiency, 1%.[14]

It was found that by using a metal Cd plate as substrate, allowing the reaction with Se vapour to proceed at a temperature a few degrees above the melting point of Cd, according to:

$$M_{(liquid)} + X_{(vapour)} \xrightarrow[\text{Ar flow}]{\Delta} MX_{(solid)} \qquad (1.13)$$

The synthesis of polycrystalline CdSe semiconductor layers with a 6.9% conversion efficiency is obtained.[15] It also enables with the use of a proper cooling system, synthesis of polycrystalline CdTe.

CHAPTER 2

EXPERIMENTAL

2.1 Cadmium Substrates

2 x 2 cm^2 cadmium substrates were cut from a 1mm thick plate of Cd 99.999% (JOHNSON MATTHEY). The substrates had been carefully cleaned with acetone and then etched for 5 seconds in a 5:4:1 mixture of H_2O:HCl:HNO_3 to provide a slight surface roughness. After that they were thoroughly rinsed with deionized water followed with methanol, and then quickly dried with nitrogen before being introduced in the reaction chamber.

2.2 Muffle Furnace and Reaction System

The liquid metal-vapour reaction system is illustrated in Figure 2.1.

(1) Reaction chamber (quartz or pyrex).

(2) Reaction chamber outer tube, extending to the exterior of the muffle furnace through hole in muffle furnace door.

(3) Hole in the center of muffle furnace door

(4) Muffle furnace door (reaction chamber can be removed or introduced in muffle furnace by pulling back or pushing forward the muffle furnace door which is guided by 2 parallel metal rods attached to the furnace).

(5) Muffle furnace (specifically designed for these experiments, equipped with a programmable microprocessor temperature control, 1 zone).

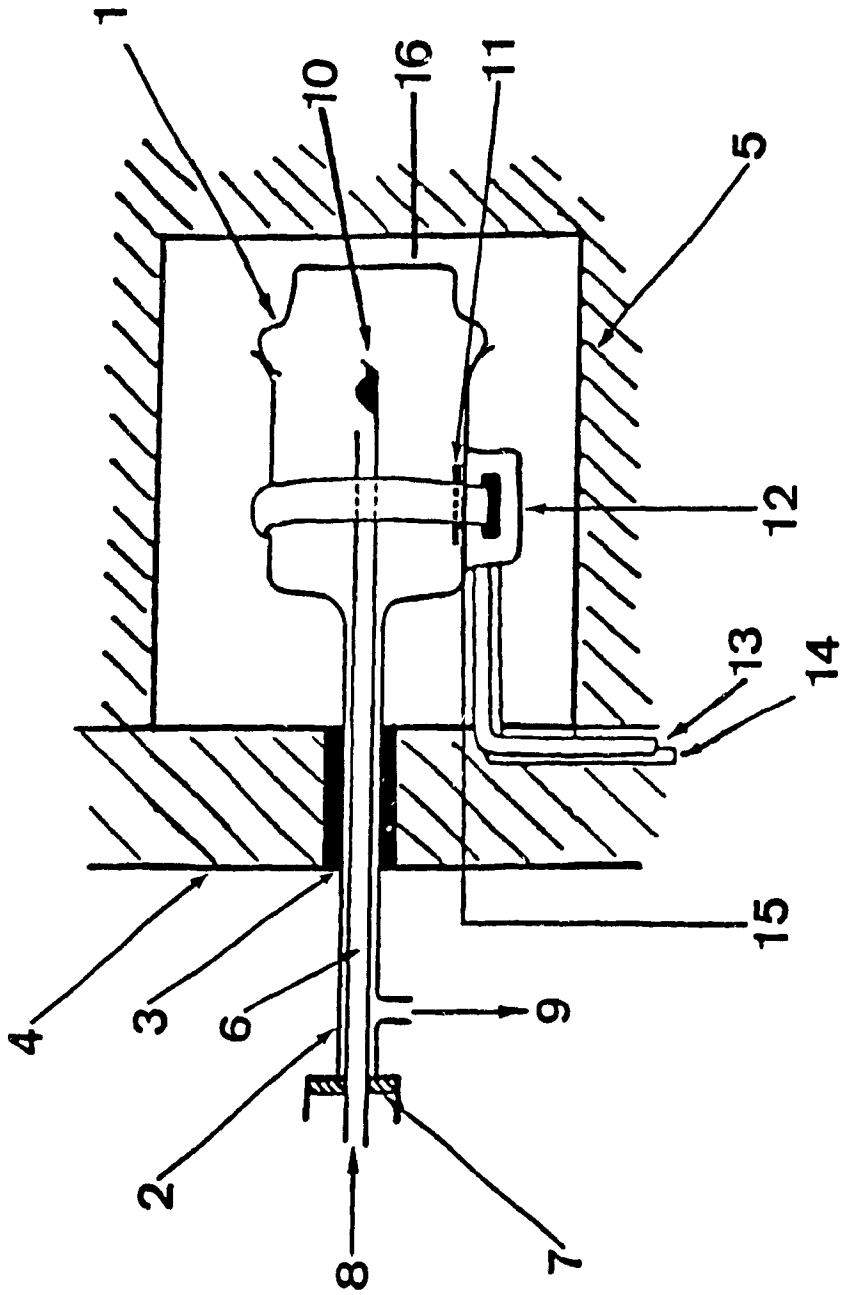

Figure 2.1 Liquid metal-vapour reaction system.

(6) Inner tube (quartz or pyrex, acts simultaneously as gas inlet and as the spoon containing selenium or tellurium).

(7) Torion sliding joint (enables the inner tube to be retracted from the reaction chamber to position the selenium or tellurium source outside the muffle furnace, while the reaction chamber is kept inside the muffle furnace).

(8) Argon inlet.

(9) Argon outlet.

(10) Selenium or Tellurium source.

(11) Cadmium substrate.

(12) Stainless steel cooling source.

(13) Water inlet.

(14) Water outlet.

(15) Thermocouple.

(16) Thermocouple of muffle furnace.

(12) - (15) are used to produce CdTe only.

To remove oxygen, the reaction chamber containing a Cd substrate is purged for 30 min (100 cm^3/min) with ultra-high purity argon (99.999%) which has passed through an Oxysorb oxygen removal unit (SPECTREX). The argon is introduced via a 0.25 inch glass tube which acts simultaneously as the gas inlet and as the spoon containing the Se or Te shot (VERTRON 99.999%). The reaction chamber is placed into the muffle furnace (PYRADIA, equipped with a programmable REX P-100 microprocessor temperature control), and the Ar flow is reduced to 35 cm^3/min.

2.3 To Produce CdSe:

Cd substrate is then heated to 325 °C (melting point of Cd is 321 °C) in the furnace within 30 min, and the reaction proceeds as the Se vapour (melting point of Se is 217 °C, the vapour pressure of Se is 0.3 mmHg at 325 °C[16]) is brought in contact with constant Ar flow, with the liquid Cd surface. The reaction is allowed to proceed for four hours. As previously reported,[17] this is the reaction time required to attain maximum thickness of 3 to 4 μm. After reaction, the CdSe sample is allowed to regain room temperature under Ar atmosphere.

2.4 To Produce CdTe:

The oven is heated to 500 °C within 1 hour while the Cd plate is maintained to 325 °C by a joint stainless steel cooling system placed beneath the metal, and controlled by water flow (Figure 2.1). This cooling system consists of a stainless steel joint, which attaches to the Pyrex reaction chamber, with extending tubes that are attached to a water tap. Between the joint and reaction chamber, there is a thermocouple (OMEGA HH-52) which monitors the Cd plate temperature. This allows both the Cd substrate and the Te source to be maintained at temperature above their respective melting points (melting point of Te is 450 °C, the vapour pressure of Te is 0.3 mmHg at 500 °C[16]) in order for the reaction to proceed. The rest of the procedure is the same as that described for CdSe.

2.5 Electrode Preparation

Once the optimized conditions reported in sections 2.3 and 2.4 were obtained, 10 samples of each material, CdSe and CdTe, were used to fully investigate the surface properties, the crystalline properties, and the overall electrochemical photovoltaic behavior.

A copper wire was attached with tin solder to the back ot the semiconductor CdX sample. The electrode and wire were stuck to a 2.5" x 1" microscope glass slide with epoxy, leaving an about 1 cm^2 of the CdX electrode exposed to the electrolyte.

2.6 Photoelectrochemical Measurement System

The whole system is shown in Figure 2.2. The white light source was used a KODAK (Model 4200) slide projector. Monochromatic excitation was obtained by using a BAUSCH & LOMB monochromator with a 10 (nm) pass. Light intensities were measured with an OPTIKON 88XLC photometer. Infrared radiation was filtered out by passing the light through a 12 cm water filter placed between the light source and the focusing lens.

Electrochemical and photoelectrochemical measurements were performed under potentiostatic control with a three electrode cell using the CdX semiconductor electrode as working electrode, a saturated calomel electrode as reference and a platinum foil (6 cm^2) as counter electrode. The quartz cell had a flat window, allowing a 3 mm optical path length through the electrolyte to the working electrode.

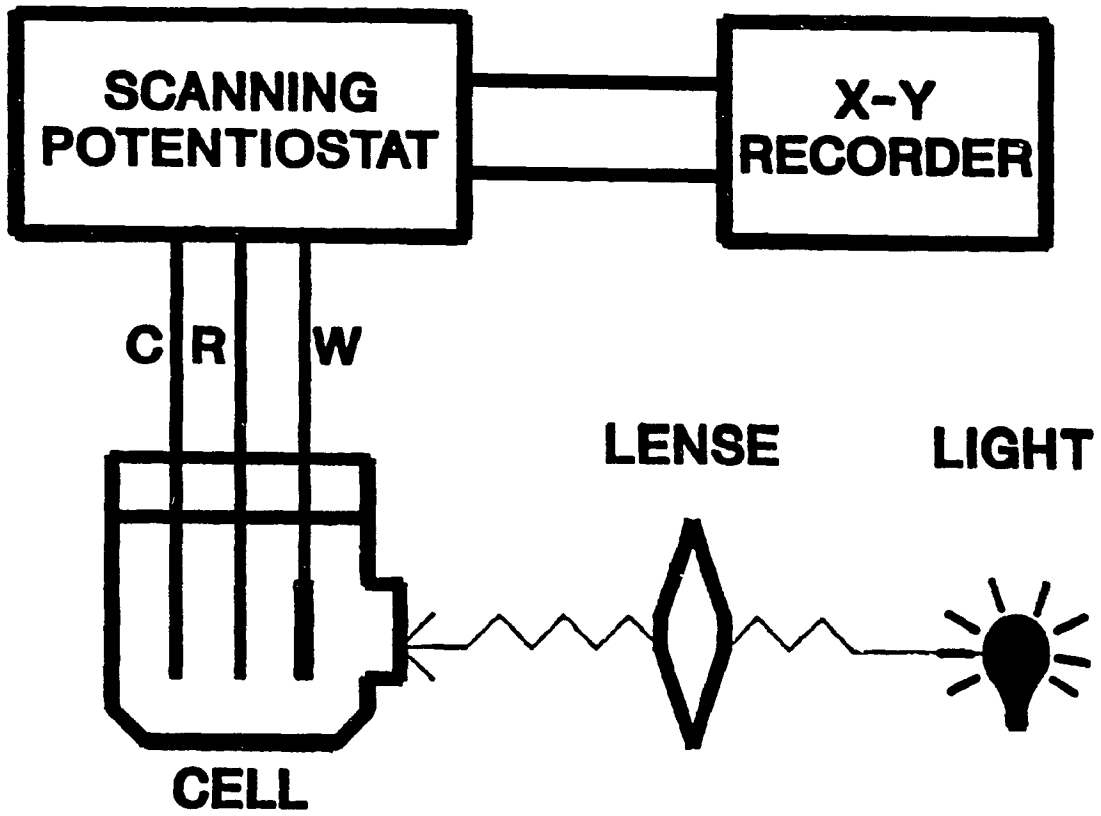

Figure 2.2 Photoelectrochemical measurement system. W = Working electrode; C = Counter electrode; R = Reference electrode.

Potentials were controlled with an EG&G Princeton Applied Research (Model 362) scanning potentiostat with output to a PHILIPS PM 8143 X-Y recorder. Photocurrent measurements were monitored by a KEITHLEY 617 programmable electrometer. The electrolyte was an aqueous polysulfide solution of composition 1M (Na_2S/S/NaOH). All the solutions were prepared from deionized water and analytical grade reagents. All measurements were performed at room temperature.

2.7 Other Instruments

The CdX layers were analyzed by scanning electron microscopy (SEM), Energy dispersive analysis of X-rays (EDAX) (HITACHI SEM Model S-570), and X-ray diffractometry (SIEMENS D-500, Cu Kα: 1.5406 Å) at Hydro-Quebec energy research center (IREQ) in Varennes. The capacitance measurements were obtained with a PAR 173 potentiostat in coupled to a 5206 lock-in amplifier, both controlled by an Apple IIe computer at I.N.R.S.-Energie in Varennes. A 10 mV peak to peak, 10 kHz a.c. voltage was used to get the capacitance values.

CHAPTER 3

RESULTS AND DISCUSSION 1

PHYSICAL AND CHEMICAL CHARACTERIZATIONS OF ELECTRODES

3.1 Scanning Electron Micrographs

Figure 3.1 presents a scanning electron micrographs (SEM) of a typical CdSe film obtained after 4 hours of reaction time. To the naked eye the surface of such a sample appears heavily textured and pitch black. Etching off the CdSe layer by applying a negative over potential (-3 V vs SCE) on the electrochemical cell reveals a Cd substrate with the same topography (Figure 3.1A) which may indicate that this crumpled texture is induced by stress during the cooling of the sample. The linear thermal expansion coefficient is 30 x 10^{-6} K^{-1} for Cd and about 2 x 10^{-6} K^{-1} for CdSe and CdTe.[12] At a magnification of 25,000, the layer surface appears as an agglomeration of crystallites with diameters ranging from approximately 0.3 to 1.0 μm

The SEM photograph in CdTe (Figure 3.2) shows the heavily textured surface of the CdTe samples which also appear pitch black. At low magnification (50x), it is similar to the CdSe topography. But at 200 magnification, a typical picture of crevices is shown. The photograph at 8,000 times is focused on a portion of the crevice, which shows an agglomeration of crystallites with diameters ranging approximately 0.3 to 2.0 μm.

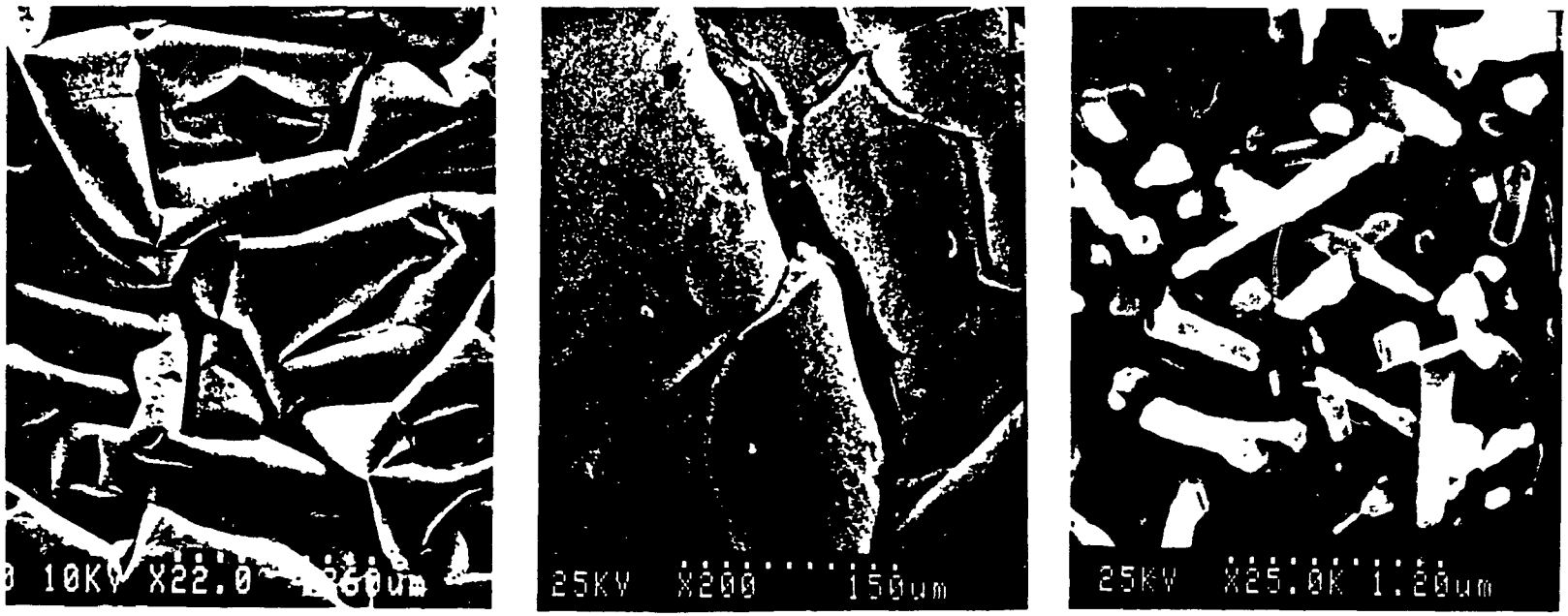

Figure 3.1 Scanning electron micrographs of CdSe.

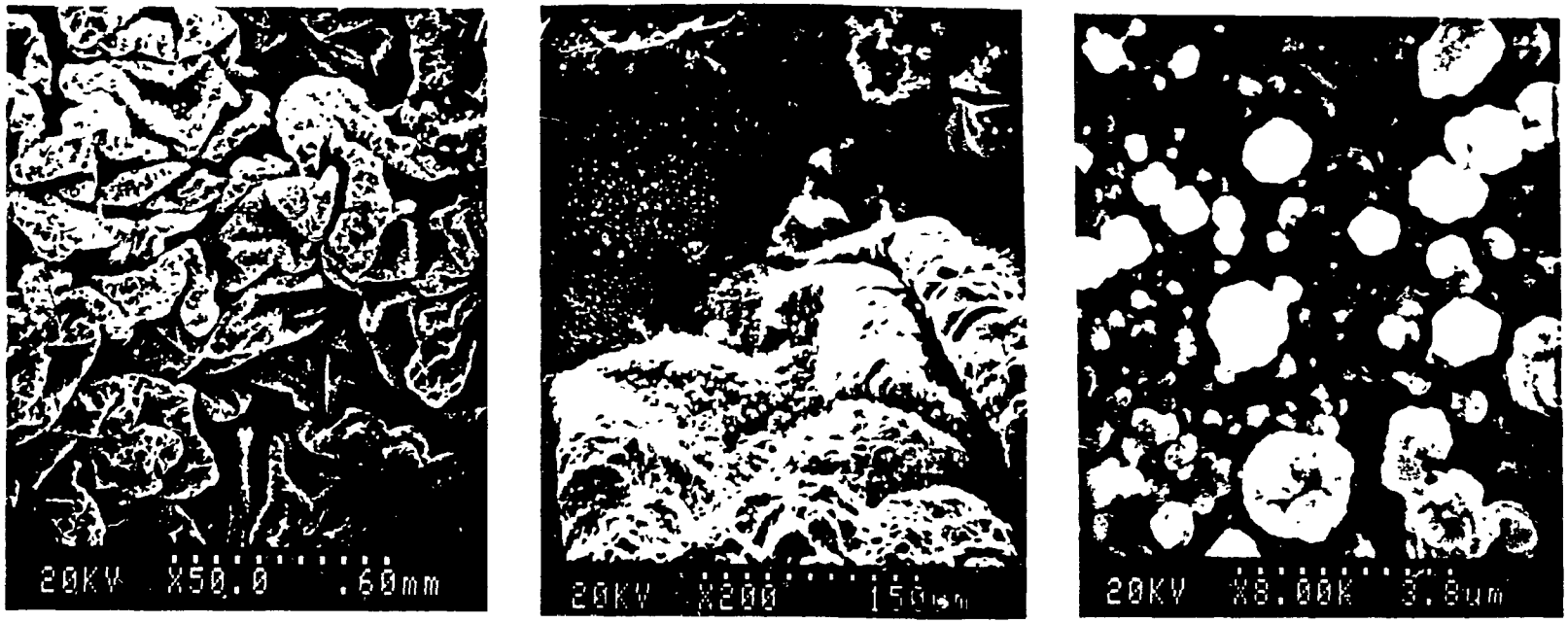

Figure 3.2 Scanning electron micrographs of CdTe.

3.2 X-ray Diffraction Patterns

The identification of a species' crystalline structure from its x-ray diffraction pattern is based upon the position of the lines (2θ) and their relative normalized, integrated intensities. The diffraction angle 2θ is determined by the spacing between a particular set of planes, using the Bragg law:

$$2\ d \sin\theta = n\lambda \qquad (3.1)$$

where n is the order of the diffraction line and is numerically equal to the path difference for successive planes; λ is wavelength; d is the interplanar spacing of the diffracting planes; and θ the bragg angle, θ is the angle between the incident x-ray and the diffracting planes.

The cadmium chalcogenides are all tetrahedrally bonded solids. X-ray diffractions performed on these polycrystalline samples indicate that the positions (2θ degrees) of the observed diffraction peaks correspond reasonably well to those reported in the JCPDS (Joint Committee on Powder Diffraction Standards) file with CdSe crystallizing in the hexagonal (wurtzite) structure (Figure 3.3), and CdTe in the cubic (zinc blende) structure (Figure 3.4). But their normalized integrated intensities, however, show little correlation. This is due to the fact that some orientations are favoured over others during formation of the CdX layer. The results of x-ray diffraction patterns are shown in Table 3.1 and Table 3.2.

It should be noted that a few of the peaks appearing in the diffraction pattern of the CdTe samples were not identified, eventhough they were compared to the standard patterns of Cd, Te, their oxides, and all possible compounds formed from these elements, which appear in the JCPDS files.

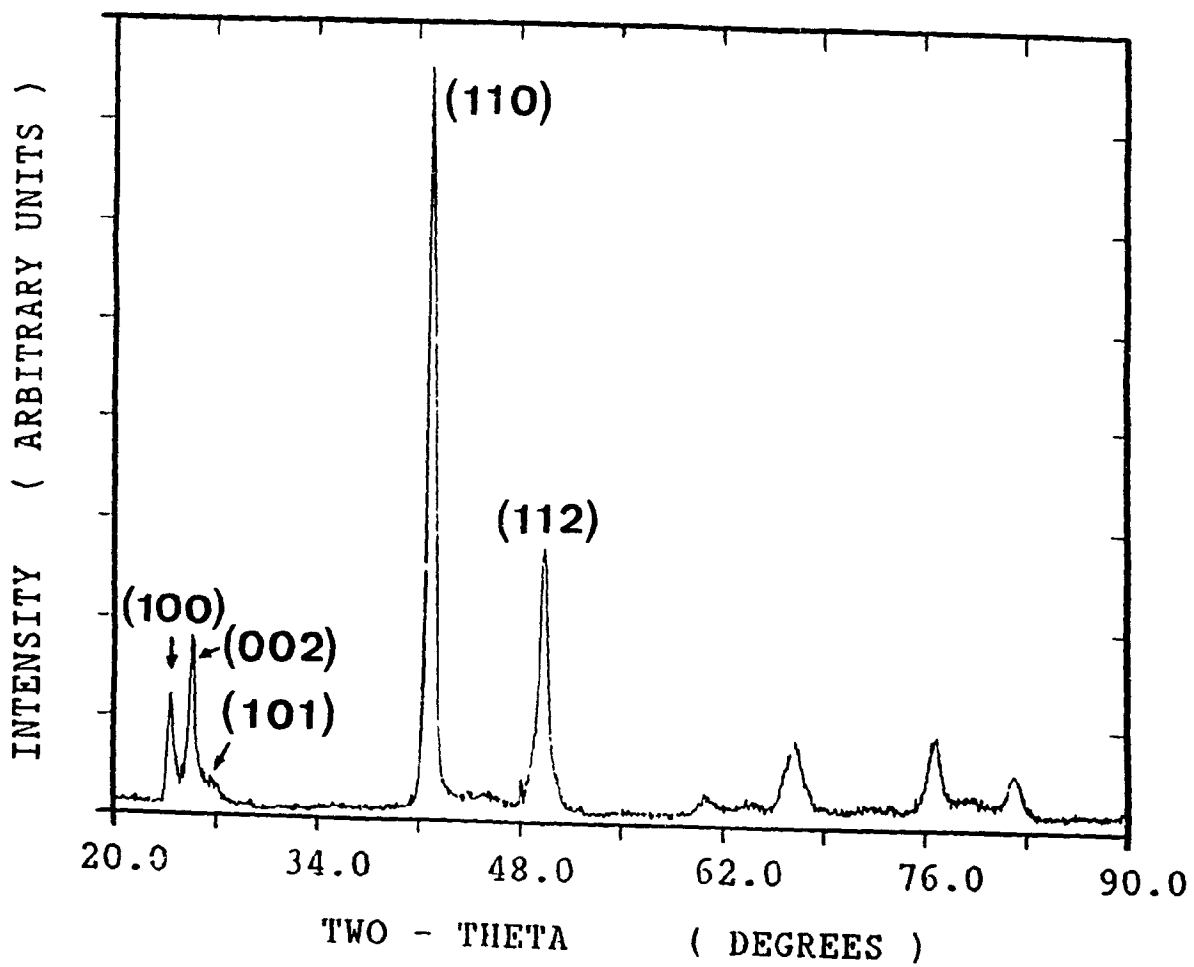

Figure 3.3 X-ray diffraction diagram of CdSe.

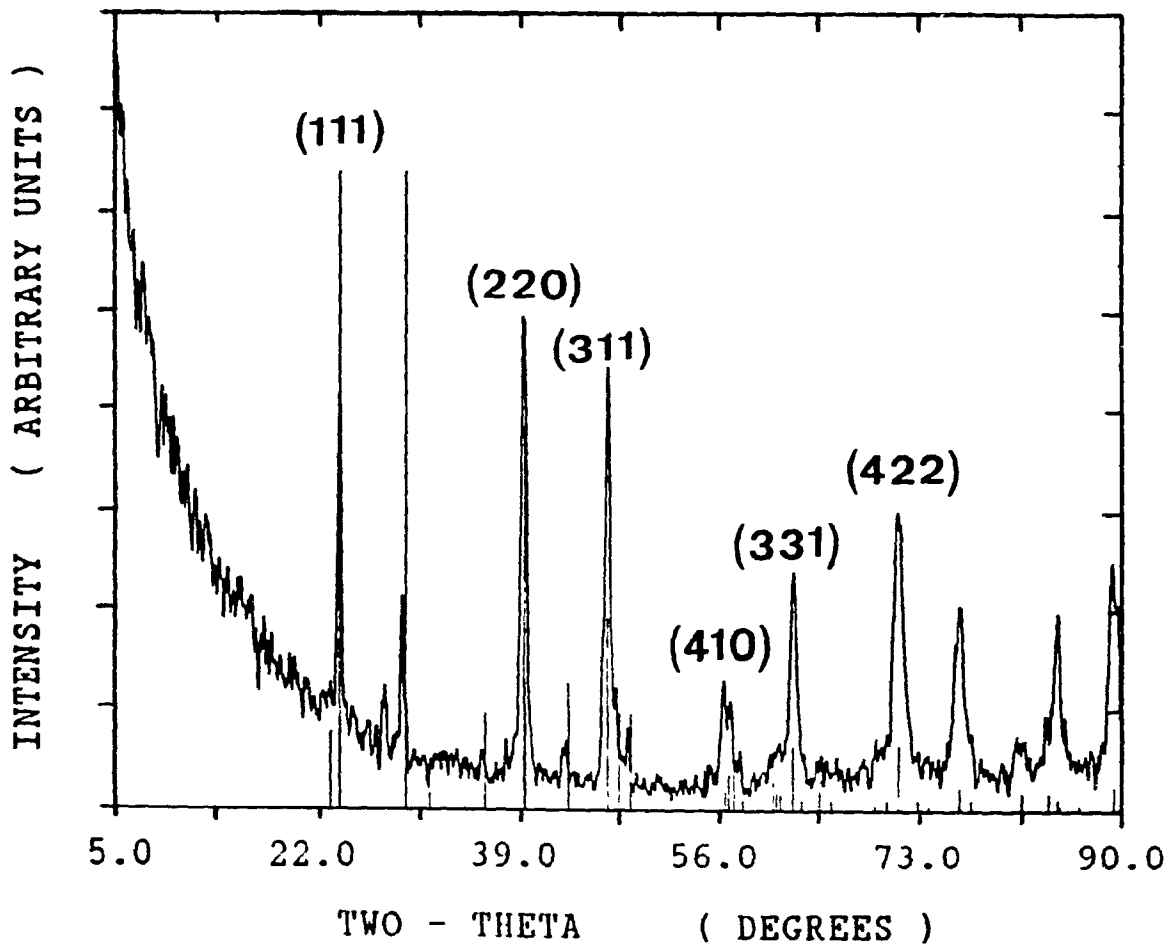

Figure 3.4 X-ray diffraction diagram of CdTe.

2θ	Experimental		JCPDS Hexagonal		
Degree	D(Å)	I%	D(Å)	I%	Plane
23.859	3.7265	11.5	3.7175	100	(100)
25.319	3.5149	13.7	3.5088	70	(002)
26.688	3.3376	0.4	3.2895	75	(101)
41.843	2.1572	100.0	2.1505	85	(110)
45.782	--	--	1.9802	70	(103)
49.582	1.8371	48.3	1.8346	50	(112)

Table 3.1 X-ray diffraction pattern of polycrystalline CdSe

2θ	Experimental		JCPDS Cubic		
Degree	D(Å)	I%	D(Å)	I%	Plane
23.754	3.7426	41.5	3.742	100	(111)
39.265	2.2926	87.6	2.290	60	(220)
46.439	1.9538	100.0	1.954	30	(311)
56.498	1.6275	20.0	1.619	6	(410)
62.475	1.4853	46.2	1.488	10	(331)
71.182	1.3235	81.0	1.323	10	(422)

Table 3.2 X-ray diffraction pattern of polycrystalline CdTe

3.3 Energy Dispersive Analysis of X-rays

The energy dispersive analysis of X-rays (EDAX) measurements indicate that the CdSe and CdTe forming these layers are richer in Cd. The atomic and weight percentages are given in Table 3.3.

Such high excesses in Cd may be due to the fact that the reaction proceeds by the diffusion of interstitial metal atoms through the chalcogenide thin film formed at the onset.[11,12] It is, therefore, possible that the percentage of Cd increases in going from the surface to the bulk of the sample, since the Se only reacts with the Cd on the surface. It should also be noted that the precise thickness of the CdX layer is difficult to assess and the coverage of the Cd substrate may be somewhat non-uniform.

		Atomic %	Weight %
CdSe	Cd	53.27	61.88
	Se	46.73	38.12
CdTe	Cd	61.63	58.27
	Te	38.69	41.73

Table 3.3 Atomic and Weight percentages of each element in CdSe and CdTe.

CHAPTER 4

RESULTS AND DISCUSSION 2

PHOTOELECTROCHEMICAL MEASUREMENTS

Much effort has been directed towards developing new and better solar energy conversion devices with efficient, cheap and stable chemical systems. In the 1970s, an alternative strategy was suggested in which a solid-liquid junction was used instead of the solid-solid junction of conventional solar cells, that is the so called electrochemical photovoltaic cell. A semiconductor electrode dipped in a liquid electrolyte provided the necessary charge transfer, a redox ionic species being used to obtain photovoltage / photocurrent. In this case, the cell offers the possibility of both solar energy conversion and storage.

All the experimental measurements in this chapter were performed with a three electrode cell under potentiostatic control using a CdX specimen as the working electrode in contact with a 1M polysulfide aqueous solution (Figure 2.2).

4.1 Capacitance Measurements

Once the semiconductor is dipped into the electrolyte, a junction is produced. The junction capacitance C is defined as the differential capacitance presented by the junction when a small a.c. voltage of amplitude dV_A is superimposed on the applied d.c. voltage V_A:

$$C = \frac{dQ}{dV_A} \qquad (4.1)$$

The analogy to the parallel-plate capacitor:

$$C = \frac{A\varepsilon\varepsilon_0}{d} \tag{4.2}$$

Where A is the junction area, ε is the semiconductor's dielectric constant (ε=10 for CdSe and ε=11 for CdTe)[18], ε_0 = 8.86 x 10^{-12} F/m, d is the distance of parallel plates apart which equals the semiconductor depletion layer.[19]

$$W = \left[\frac{2\varepsilon\varepsilon_0 \left(V_A - V_{fb} - \frac{kT}{q}\right)}{qN_D} \right]^{0.5} \tag{4.3}$$

where q is the electronic charge, k is the Boltzman constant, T is the absolute temperature, A is the sample area in contact with the electrolyte, V_A applied potential, and V_{fb} flat band potential.

The well known Mott-Schottky relation is the combination of Equation 4.2 and Equation 4.3,

$$\frac{1}{C^2} = \frac{2}{\varepsilon\varepsilon_0 q N_D A^2} \left(V_A - V_{fb} - \frac{kT}{q}\right) \tag{4.4}$$

Equation 4.4 is based on the assumption that the semiconductor-electrolyte interface can be treated as three capacitances in series: the semiconductor depletion region, the Helmholtz layer, and the Gouy layer (Figure 1.4). At high ionic concentration (1M) in the electrolyte, q in the electrolyte is much more than in the depletion region. The capacitance of the Gouy layer and helmholtz layer are much larger than that of the depletion region. In series,

$$\frac{1}{C_{Total}} = \frac{1}{C_D} + \frac{1}{C_H} + \frac{1}{C_G} \qquad (4.5)$$

So that capacitances of the Gouy layer and the Helmholtz layer can be neglected, and equation 4.4 can be used to investigate the semiconductor depletion region.[20]

Figure 4.1 and Figure 4.2 present the variations of depletion region capacitance C, as a function of applied potential V_A, which enable the determinations of the semiconductor's majority charge carrier density N, and flatband potential V_{fb}. For an ideal system, a plot of C^{-2} versus electrode potential yields a straight line with an intercept at $C^{-2} = 0$ equal to V_{fb}, and a slope related to the carrier density. But these directly measured values have to be corrected for the real as opposed to apparent surface area of the electrodes using a roughness factor estimated from inspection of SEM photographs and BET test. Assuming this factor is 5 one obtains an estimate doping of the actual density. All results are shown on Table 4.1 below. These results were found to be frequency independent in the range of 5 to 20 kHz.

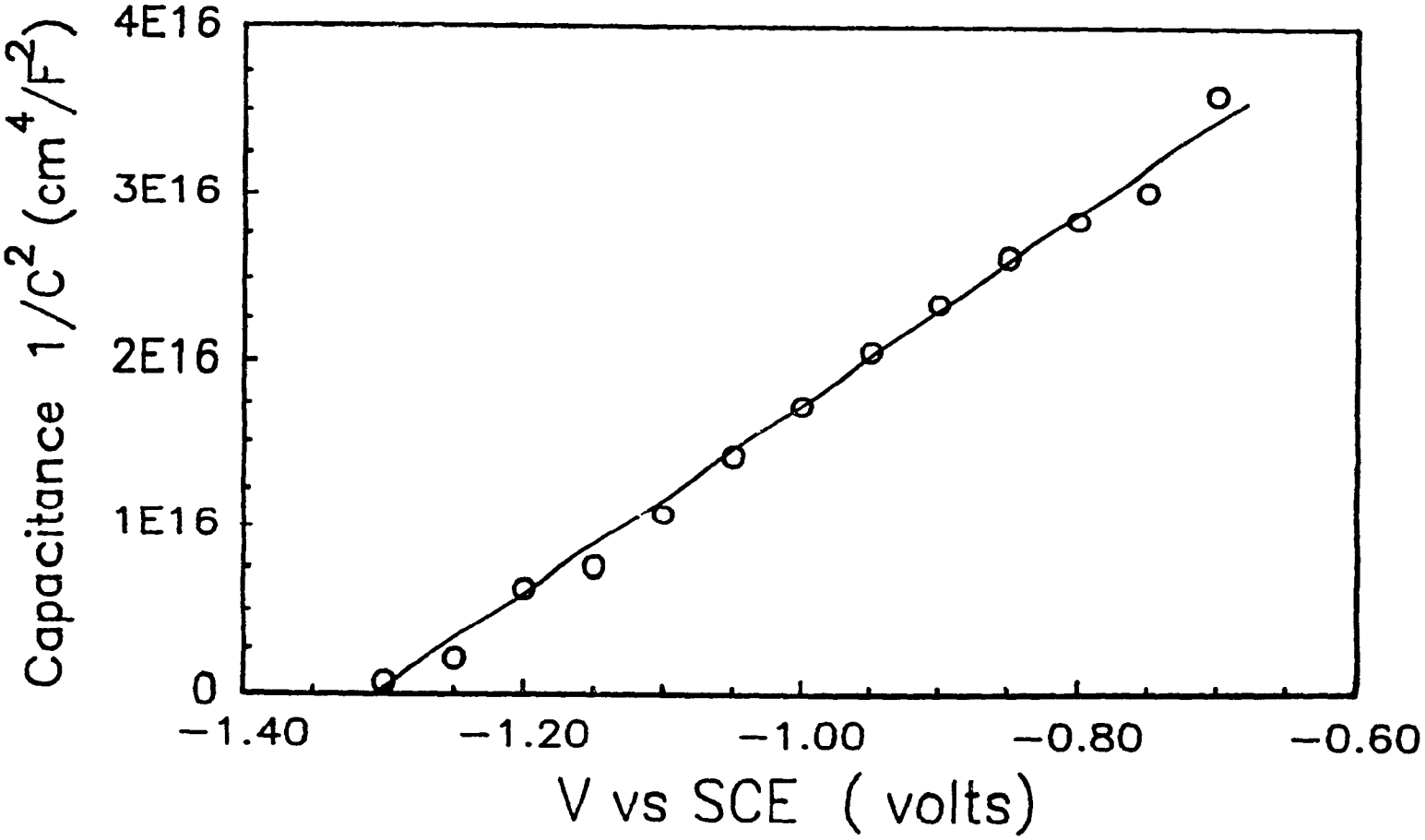

Figure 4.1 Mott-Schottky plot of CdSe.

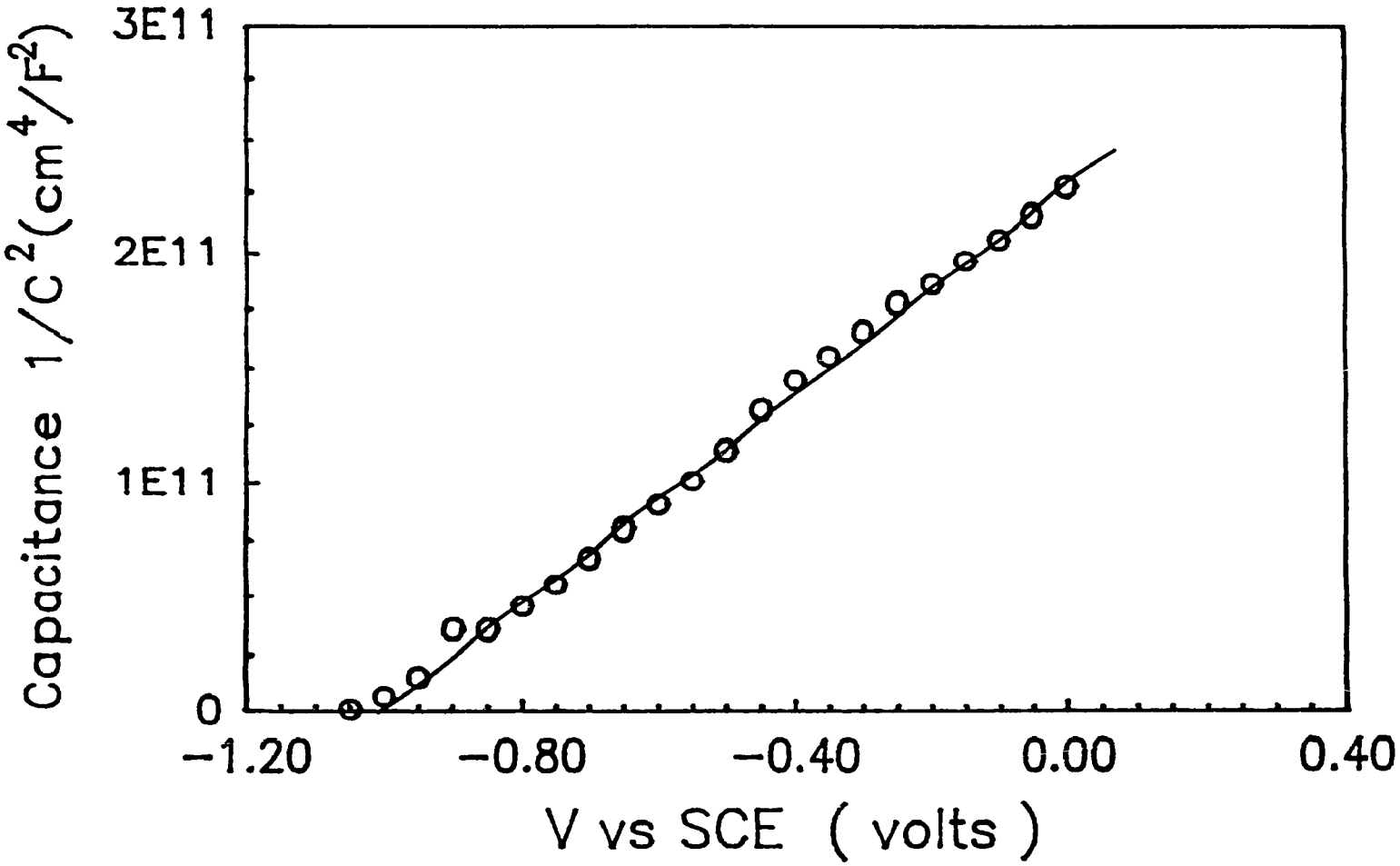

Figure 4.2 Mott-Schottky plot of CdTe.

	V_{fb}	N_D	Estimated real N_D
CdSe	-1.31 V vs SCE	2.6×10^{17} cm^{-3}	5.2×10^{16} cm^{-3}
CdTe	-1.02 V vs SCE	7.8×10^{19} cm^{-3}	1.6×10^{19} cm^{-3}

Table 4.1 Flat band potentials and doping denisities of CdSe and CdTe.

4.2 Current-Voltage Characteristics

The current-voltage characteristic of CdSe shown in Figure 4.3 were obtained in a three electrode cell under 80 mW/cm^2 of white light illumination. The voltage applied to the semiconductor working electrode was varied from +0.3 V to -1.7 V vs standard calomel electrode (SCE), and the cell yields:

A short-circuit photocurrent density

$$J_{sc} = 22 \text{ mA/cm}^2 \text{ at } V = V_{redox} = 0.75\text{V vs SCE,}$$

An open-circuit photovoltage

$$V_{oc} = V_{fb} - V_{redox} = 1.31 - 0.75 = 0.56 \text{ V.}$$

The shaded area of Figure 4.3 represents the maximum power that can be derived from a solar cell. V_m and J_m are the voltage and current density at the maximum power point P_m, and the solar cell is operated at this point.

$$P_m = V_m J_m \tag{4.6}$$

Ideally a solar cell should have $V_m = V_{oc}$ and $J_m = J_{sc}$. However, various loss mechanisms operating within the cell, such as bulk recombination and interface recombination of minority charge carriers, make it deviate from the ideal behaviour. The term used to express this departure is known as the fill factor (FF) which equals 0.45 for CdSe samples, and is defined by:

$$\text{fill factor FF} = \frac{P_m}{V_{oc} J_{sc}} \tag{4.7}$$

and equation 4.6 becomes:

$$P_m = V_{oc} J_{sc} FF \tag{4.8}$$

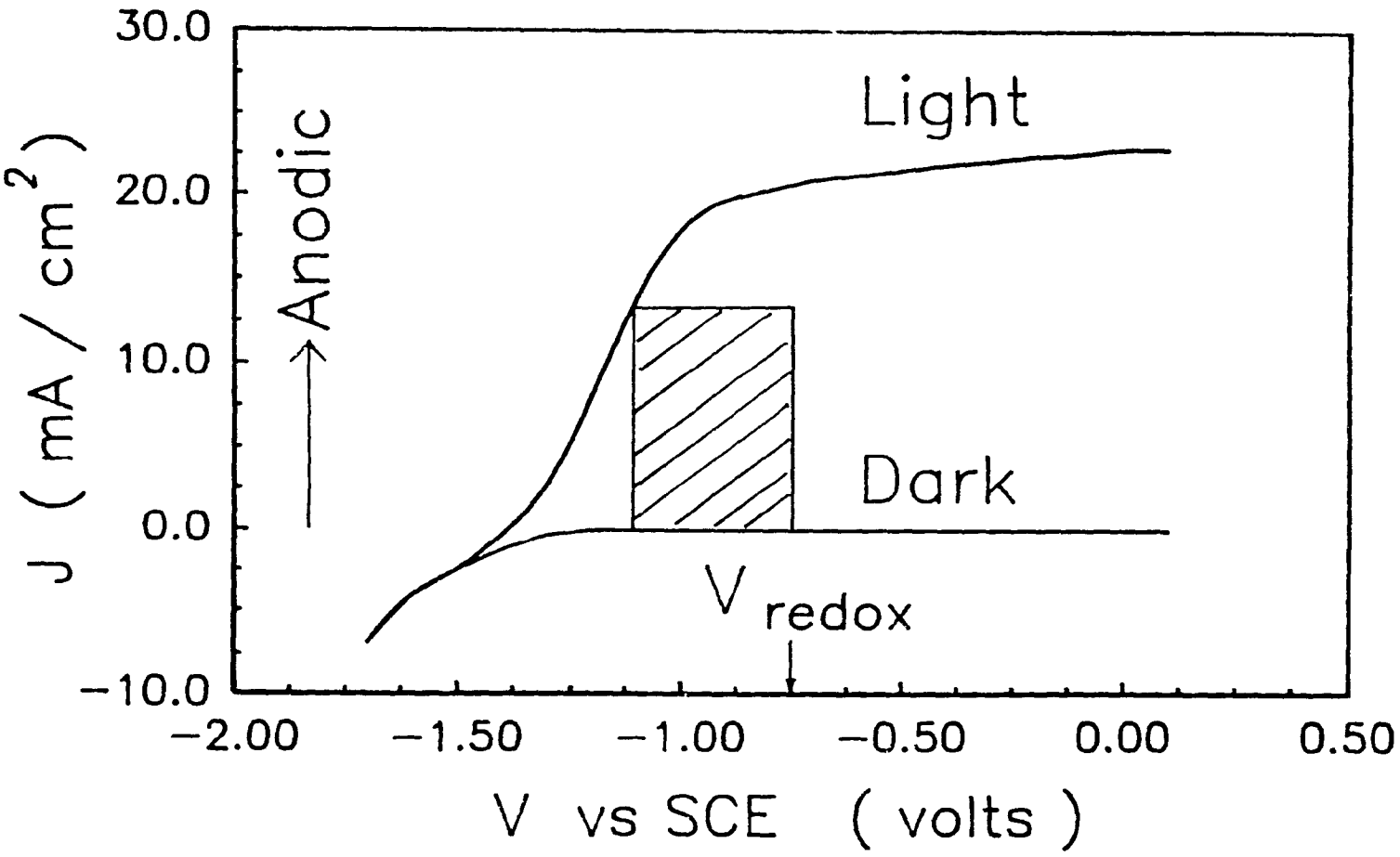

Figure 4.3 Current-voltage characteristic of CdSe.

The CdSe samples gave an overall photovoltaic conversion efficiency of η = 6.9%, as calculated according to the following equation.

$$\eta = \frac{P_m}{P_{in}} = \frac{V_{oc}\, J_{sc}\, FF}{\text{incident light power}} \qquad (4.9)$$

This value rates amongst the highest efficiencies measured under similar conditions with polycrystalline CdSe in a electrochemical photovoltaic cell.[21,22]

Figure 4.4 shows the typical current-voltage characteristic of a CdTe specimen, under the same conditions described above, expect that the white light illumination equals 48 mW/cm^2. The overall photovoltaic conversion efficiency of the polycrystalline CdTe is 0.2%.

Photocurrents for CdSe and CdTe are observed to be anodic thus indicating that both CdSe and CdTe obtained by liquid metal-vapour reaction are n-type semiconductors. From the EDAX measurements previously seen, where Cd is found to be in excess for both CdSe and CdTe samples, n-type semiconducting behaviour is expected since Cd acts as a donor. From the results of the Mott-Schottky plots, after correcting the values for the actual surface area of the samples, the doping density of CdSe is 5.2 x 10^{16} cm^{-3} while that of CdTe is 1.6 x 10^{19} cm^{-3} (Table 4.1). The CdTe sample is more highly doped, and, therefore, less photocurrent density and efficiency is expected.

The current density resulting from the net drift in the x-direction (through the layer perpendicular to its surface) is the number of electrons crossing a unit area per unit time (n $\langle v_x \rangle$) multiplied by the charge of the electron (-q):

$$J_x = - q\, n \langle v_x \rangle \qquad (4.10)$$

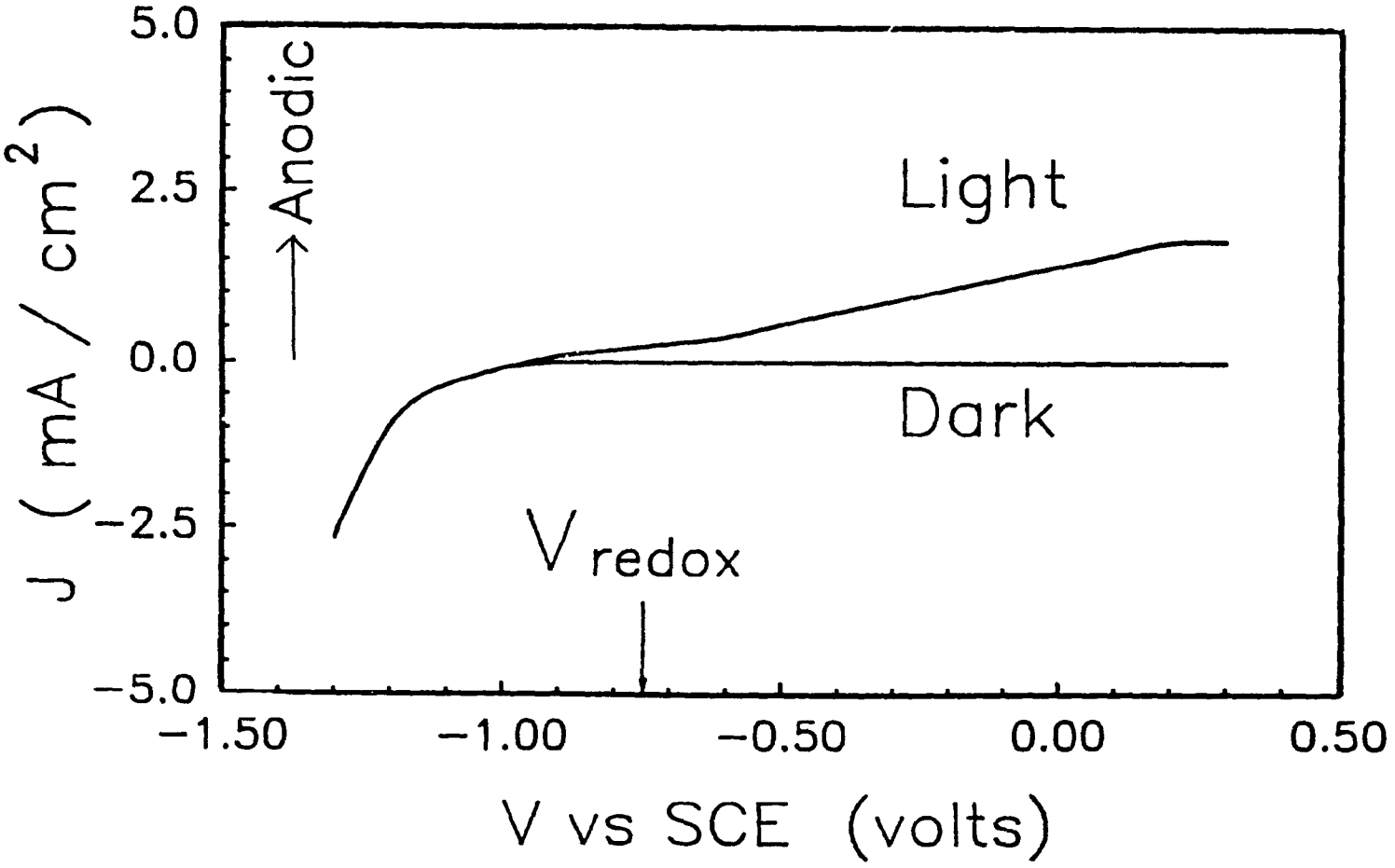

Figure 4.4 Current-voltage characteristic of CdTe.

where $\langle v_x \rangle$ is a constant net velocity in the negative x-direction.[23]

The mobility is defined as the average particle drift velocity per unit electric field.

$$\mu_n = - \frac{\langle v_x \rangle}{\varepsilon_x} \qquad (4.11)$$

For holes, p is used instead of n, and +q instead of -q. The current density can be written in terms of mobility as

$$J_x = q\, n\, \mu_x\, \varepsilon_x \qquad (4.12)$$

In most cases, as the concentration of impurities increases, the electrostatic attraction increases. Consequently the mobility of electrons or holes decreases, and therefore the measured current density is decreased.

4.3 Spectral Responses of CdX Electrodes

The short-circuit spectral responses of the electrochemical photovoltaic cells using CdSe and CdTe are shown in Figure 4.5 and Figure 4.6 respectively. The onset of photocurrent at longer wavelengths (near infrared) indicates the bandgap energy of the material. The photo response cut-off at shorter wavelengths is due to light absorption by the electrolyte.

Two calibrations have been done for photocurrent response spectra.

1) The dark current is subtracted from the current under illumination.

2) Because the incident monochromatic light has different intensities at different wavelengths, the photocurrents have been normalized for a constant photon flux.

The extrapolation of the values obtained from the measurements of photocurrent versus wavelength in the near infrared yields a bandgap energy of

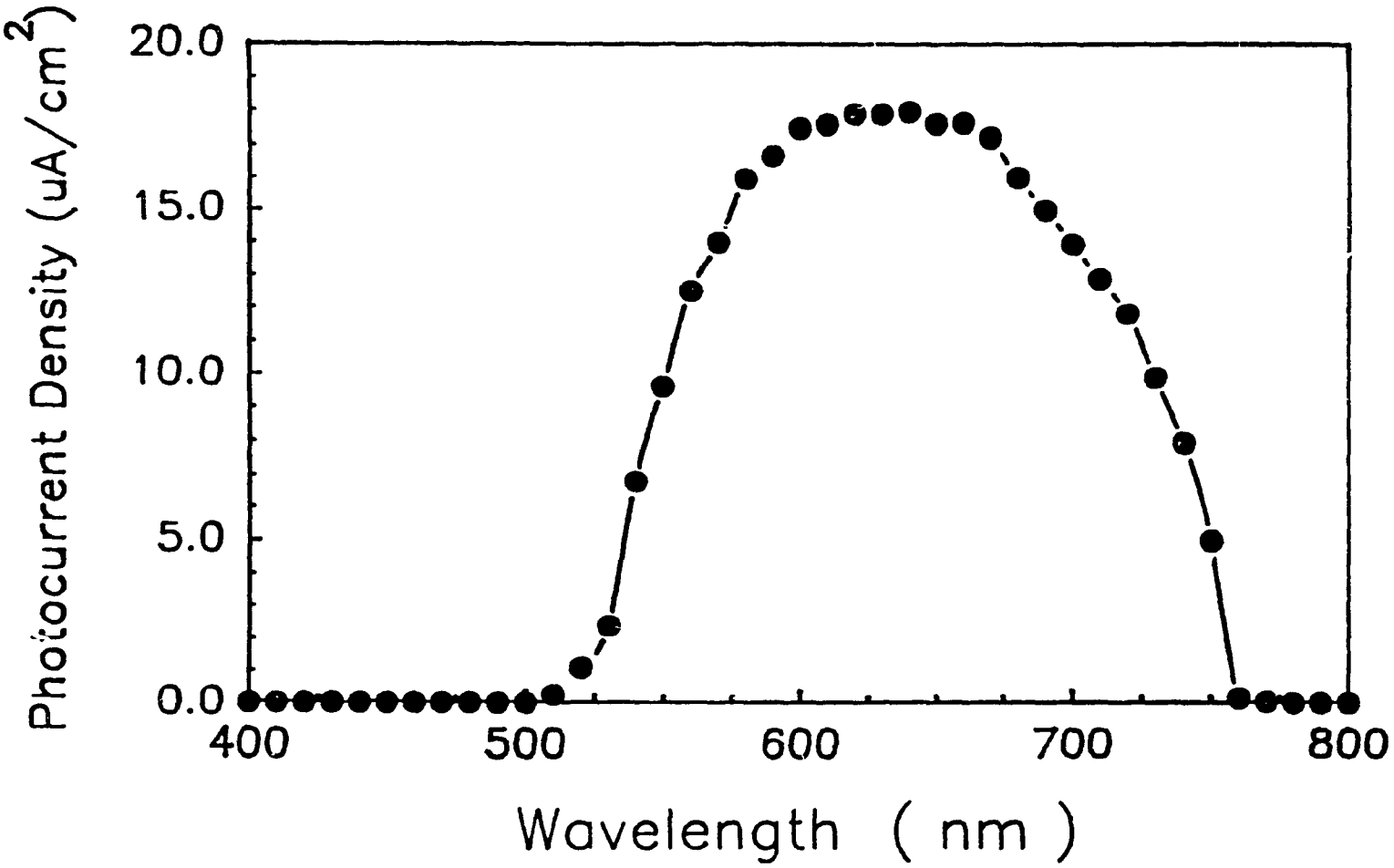

Figure 4.5 Spectral response of CdSe.

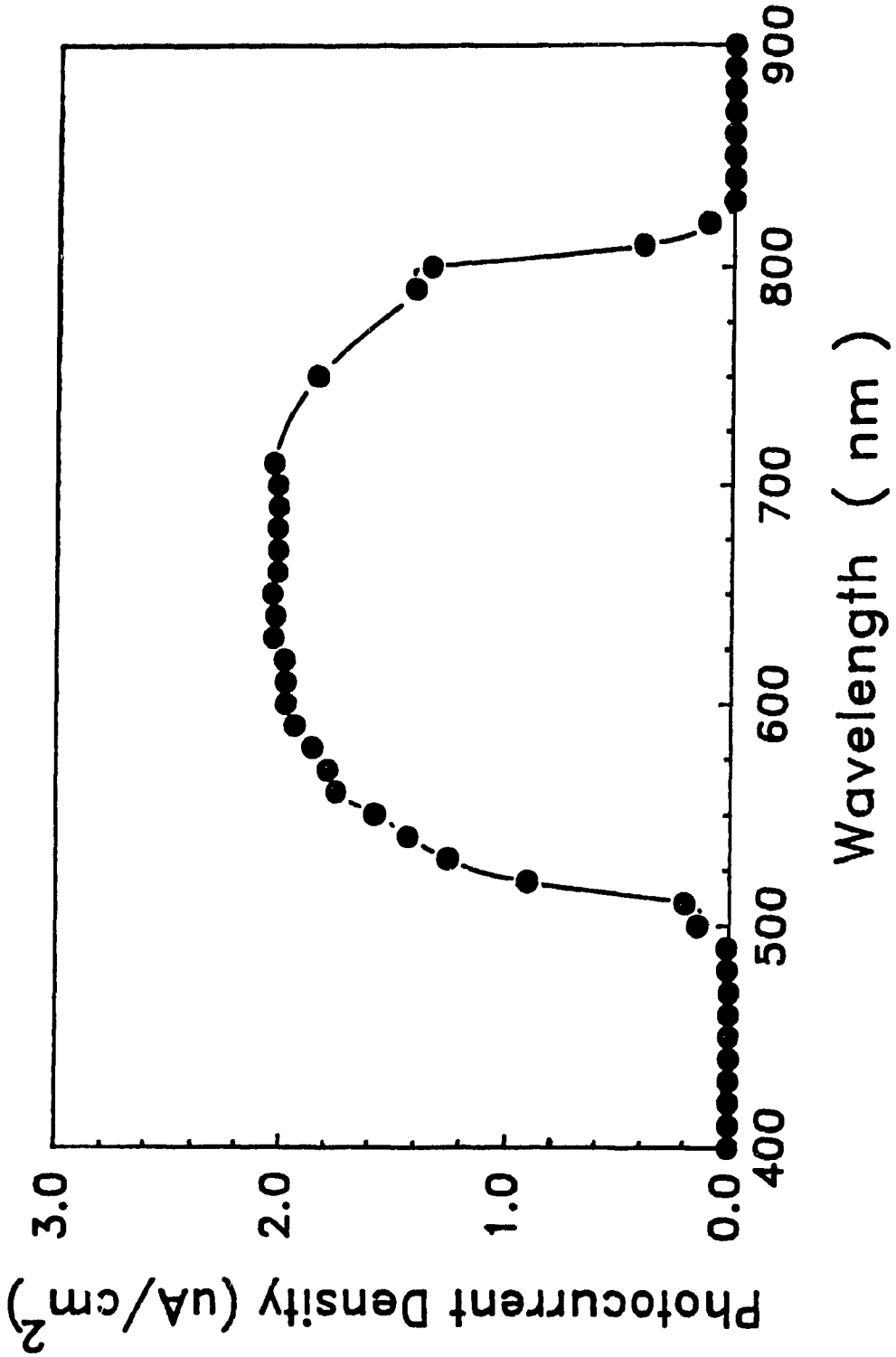

Figure 4.6 Spectral response of CdTe.

1.64 eV (755nm) for CdSe and 1.49 eV (830nm) for CdTe. These values coincide fairly well with the literature values (Table 1.1).

Theoretically, for a direct gap material like CdSe, the absorption coefficient near the absorption edge is described by[24,25]

$$\alpha = \frac{A\,(h\nu - E_g)^{0.5}}{h\nu} \qquad (4.13)$$

and the quantum efficiency is given by[26]

$$\Phi = \frac{I}{qA\phi} = 1 - \frac{EXP\,(-\alpha W)}{1 + \alpha L_p} \qquad (4.14)$$

where I is the short-circuit photocurrent, q is the electronic charge, A is the sample area, and ϕ is the incident light flux, α is the absorption coefficient, W is the depletion layer width which is given by Equation 4.3, and L_p is the diffusion length for holes.

Considering absorption coefficients such that $\alpha L_p << 1$ and $\alpha W << 1$, expansion of Equation 4.14 yields

$$\Phi \approx \alpha\,(W + L_p) \qquad (4.15)$$

Combining Equation 4.13 and 4.15, a plot of $(\Phi h\nu)^2$ vs $h\nu$ should give a straight line with intercept on the x-axis equal to the bandgap energy. This plot is shown in Figure 4.7 and Figure 4.8, and the bandgap of CdSe is found to be 1.65 eV while that of CdTe is 1.52 eV. These values are very close to the ones obtained from the extrapolations of the photocurrent responses spectra. The results indicate, as expected, that the CdSe and CdTe are direct bandgap materials. On Figures 4.7 and 4.8, one can observe a slight trailing of the data points at the onset of absorption.

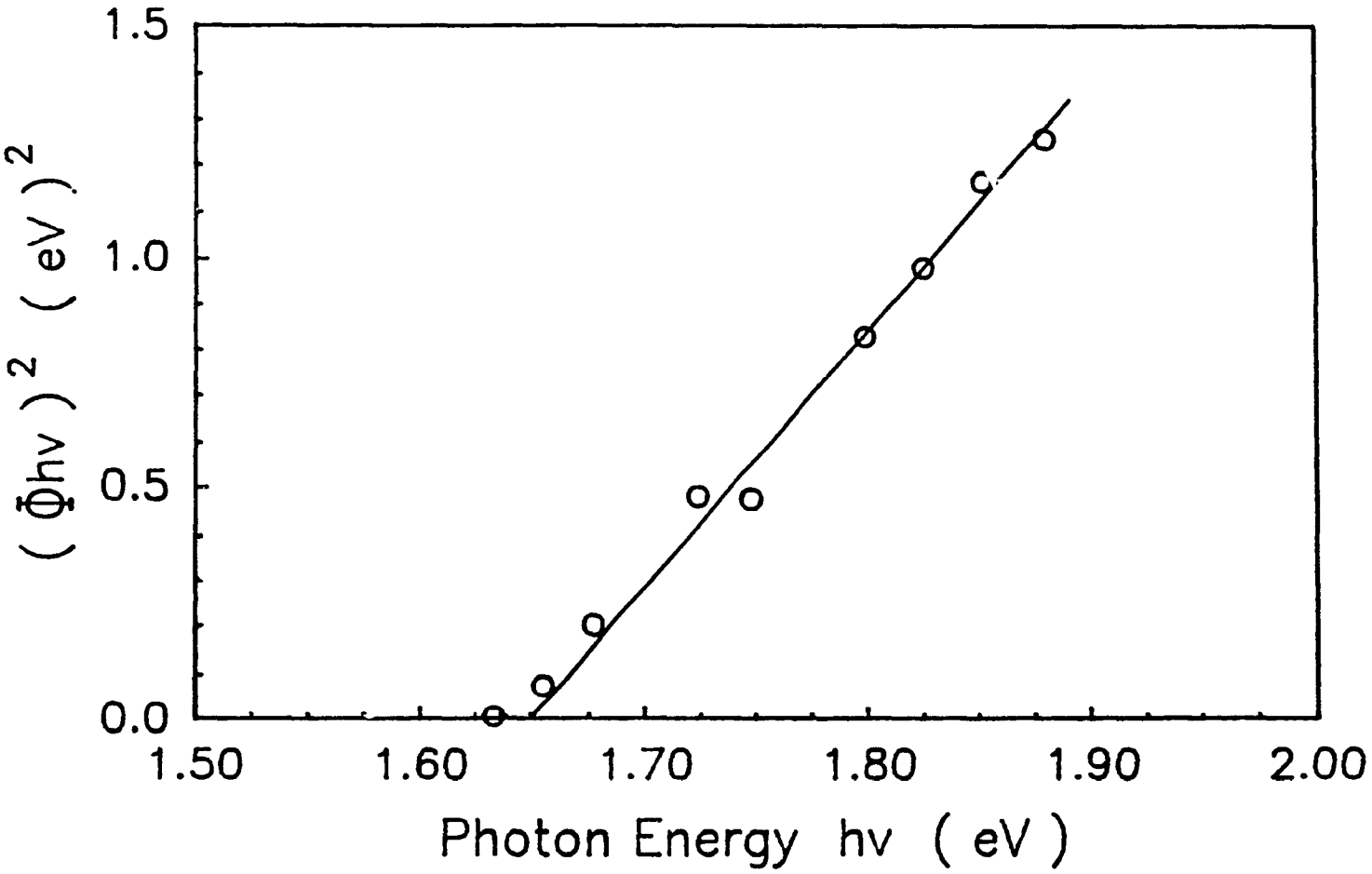

Figure 4.7 Quantum efficiency with bandgap energy diagram of CdSe.

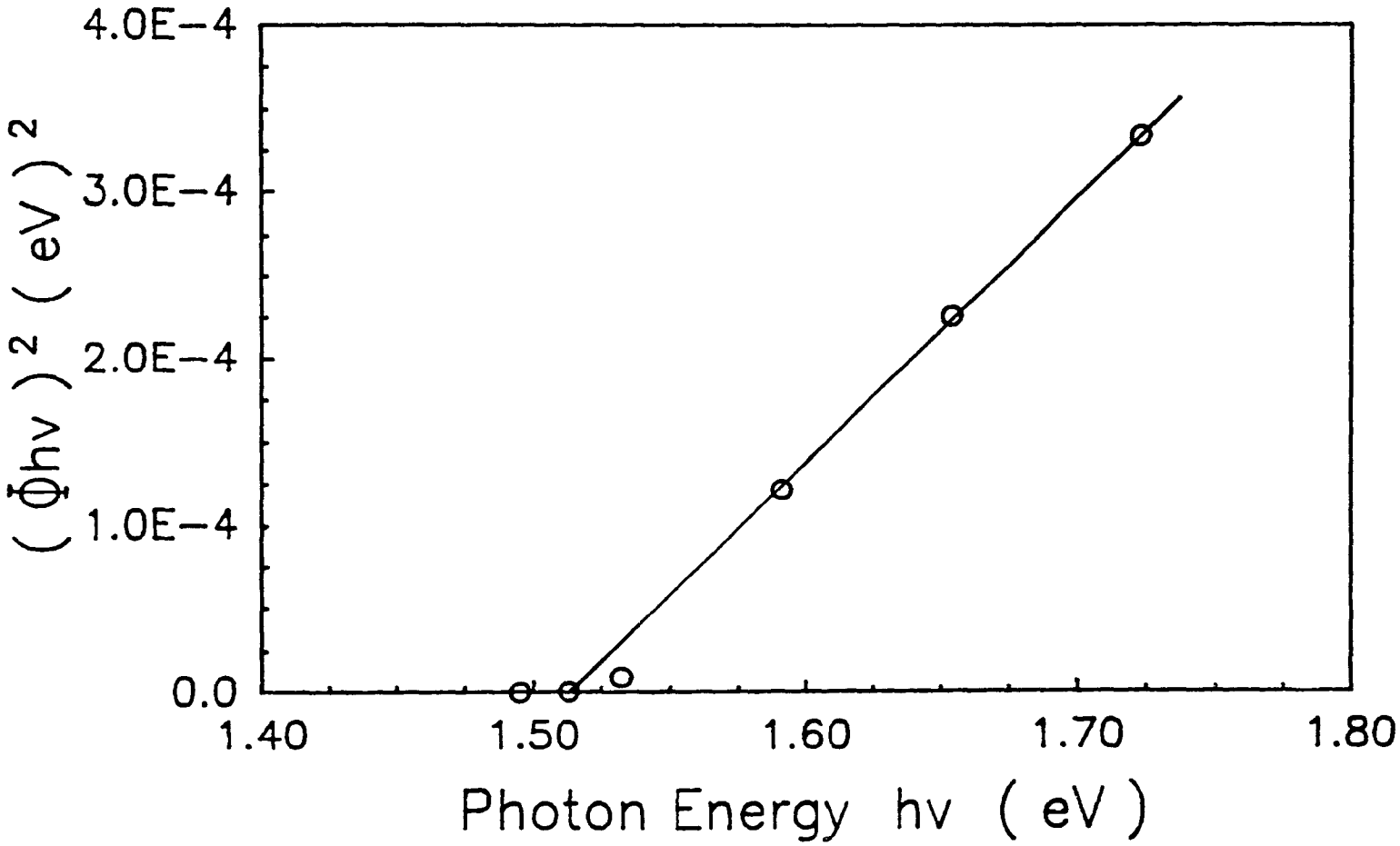

Figure 4.8 Quantum efficiency with bandgap energy diagram of CdTe.

This effect corresponds to the typical Urbach exponential tail[24] which is associated to transition probability. The low energy photocurrent onset indicates that the distribution of optically induced transition probabilities are spread out compared to single crystal CdSe and CdTe samples.[12] Because of the largely polycrystalline character of the layers grown by the liquid metal-vapour process, it should be mentioned that a possible contribution to the sub-bandgap absorption observed in Figure 47 and 48, may come from the statistically dispersed lattice imperfections, which cause the valence and conduction band levels to extend slightly one toward the other.[20]

4.4 Photocurrent Stability

Figure 4.9 presents the CdSe electrode stability in 1M polysulfide solution. After 20 hours, the photocurrent has gone down by about 20%.

Curran et al. reported that CdSe photoelectrodes produced by tarnishing reaction could be used for a number of hours, and yellowish deposits could be observed afterwards due to the replacement of CdSe by CdS from the solution. But yellowish deposits did not show up on our samples while in the polysulfide solution, instead, black solid grains (CdSe) were accumulated in the solution of the cell.

The addition of small concentrations of Se to the polysulfide electrolyte increases the stability of the CdSe polysulfide system. The surface of CdSe photoelectrodes operated in Se-containing polysulfide solution has been shown to undergo much less S/Se exchange than those operated in pure polysulfide

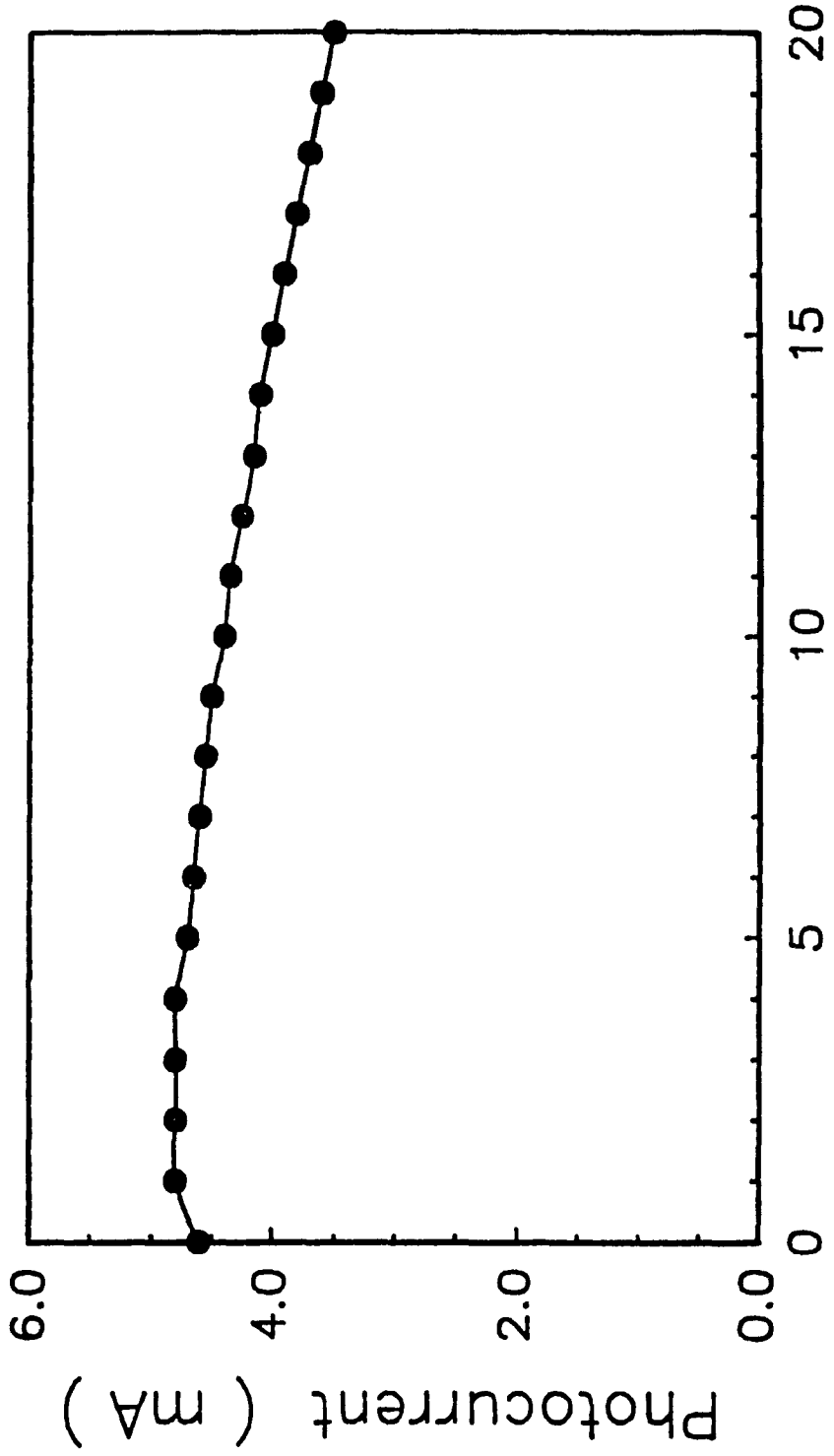

Figure 4.9 Photocurrent stability of CdSe.

solutions.[27]

The CdTe samples, on the other hand, were found to be much less stable lasting approximately two hours, which is in agreement with Ellis's report where CdTe with S^{2-}/S_n^{2-} was found to be grossly unstable.[28]

4.5 Effects of Electrolyte

The redox couples chosen should be stable in both forms as well as highly soluble to prevent mass transport limitation control of the current. They should be inexpensive and ideally neither form should absorb light of energy above E_g.[29]

Since 1976, the n-cadmium chalcogenide / aqueous polysulfide electrochemical photovoltaic cell, n-CdX/S_j^{2-} (j = 2 to 5), has been the most studied and in some ways the most promising of these liquid junction solar cells[30,31]. But despite hundreds of studies, neither the reactive chemical species nor the chemical mechanism of operation is known. The polysulfide electrolyte used in the n-CdX/S_j^{2-} electrochemical photovoltaic cell system, formed by simple dissolution of a sulfide salt, sulfur and sodium hydroxide in water, is known to be highly complex, containing H^+, H_2S and many anions OH^-, HS^-, S^{2-}, polysulfides S_j^{2-} (j = 2 to 5), supersulfide S_2^-, thiosulfate $S_2O_3^{2-}$, and sulfate SO_4^{2-}.[32,33,34] As a result of this complexity, the overall mechanism of photoinduced oxidation at the anode in the n-CdX/S_j^{2-} electrochemical photovoltaic cell system has remained unknown, but it has generally been simplified to

$$S^{2-} + 2h\nu \rightarrow S + 2e^- \qquad (4.16)$$

Licht suggested an overall mechanism for the action of CdX/S_j^2 electrochemical photovoltaic cells.[35] In both dark and photoactive environments CdX materials, when immersed in polysulfide electrolytes, exchange with sulfur at the surface first (Figure 4.10). The resultant CdS surface provides stable sites for photooxidation, and must act as a window for photon absorption in the bandgap optimised space-charge region of the semiconductor. Once electron-hole pairs are photoexcited and separated, the holes go to the solid-liquid interface, while electrons go into the bulk, through the external circuit, and reduce at the counter electrode. According to this mechanism, photocurrent is limited by supersulfide adsorption.

Licht et al. showed that CdSe in 1:1:1 polysulfide electrolyte improved in efficiency and longevity if Cs^+ is used instead of Na^+ as the cation[36,37]. The kinetics of the polysulfide electrochemical redox reactions increase in parallel with the size of the accompanying cation according to the sequence $Li^+ < Na^+ < K^+ < Cs^+$.[38] Cell efficiencies and long term stabilities go in the same order. In polysulfide solutions, the cation activity and dissolved polysulfide redox potential also exhibits this ordering.

The reason for this is the degree to which the cation is hydrated which follows the sequence Li > Na > K > Cs. Cesium ions contain little or no hydrated shell. The highly hydrated cation depresses anionic mobility and causes anion adsorption to be less. Anion adsorption should increase smoothly from lithium to cesium polysulfide. However, Cs_2S presents a major disadvantage with respect to cost-effectiveness and, therefore, its use in this work was omitted.

$$CdX_{surface} + S^{2-}_{(j+1)(aq)} \longrightarrow CdS_{surface} + XS^{2-}_{j(aq)}$$

$$S^{2-}_{4(aq)} \rightleftharpoons 2S^{-}_{2(aq)}$$

$$S^{-}_{2(aq)} + CdS_{surface}..CdX_{sc}..CdX_{bulk} \rightleftharpoons S^{-}_{2(ad)}.CdS_{surface}..CdX_{sc}..CdX_{bulk}$$

$$S^{-}_{2(ad)}.CdS_{surface}..CdX_{sc}..CdX_{bulk} + h\nu \longrightarrow S^{-}_{2(ad)}.CdS_{surface}..CdX_{sc}(h^{+}.e^{-})..CdX_{bulk}$$

$$S^{-}_{2(ad)}.CdS_{surface}..CdX_{sc}(h^{+}.e^{-})..CdX_{bulk} \longrightarrow S^{-}_{2(ad)}.CdS_{surface}(h^{+})..CdX_{sc}..CdX_{bulk}(e^{-})$$

$$S^{-}_{2(ad)}.CdS_{surface}(h^{+})..CdX_{sc}..CdX_{bulk}(e^{-}) \longrightarrow S_2.CdS_{surface}..CdX_{sc}..CdX_{bulk} + e^{-}_{external}$$

$$e^{-}_{external} + R \longrightarrow R^{-}$$

$$S_2.CdS_{surface}..CdX_{sc}..CdX_{bulk} + S^{2-}_{(j-1)(aq)} \rightleftharpoons S^{2-}_{(j+1)(aq)} + CdS_{surface}..CdX_{sc}..CdX_{bulk}$$

$$(j-1)S^{2-}_{(j+1)(aq)} + HS^{-} + OH^{-} \rightleftharpoons jS^{2-}_{j(aq)} + H_2O$$

Figure 4.10 Mechanism of polysulfide electrolyte.

The reason for choosing the polysulfide electrolyte for CdSe and CdTe semiconductors are the following:1) Se and Te electrolytes are highly coloured and increase the short wavelength photocurrent losses.

2) No significant improvement in efficiency of the CdX/Se_n^{2-} system compared to the CdX/S_n^{2-} system has been reported.

3) The extreme air sensitivity of the selenide and telluride containing electrolytes presents a stability problem for practical devices. The ways of improving on the stability of these systems are discussed in the following section.

CHAPTER 5

CONCLUSIONS AND SUGGESTIONS

5.1 Conclutions

High efficiency and relatively stable CdSe and CdTe photoelectrodes can be formed by this simple liquid metal-vapour process.

There are a number of possible reasons why the simple procedure used leads to such good results.

1) The low temperature is clearly a positive factor, as it reduces the likelihood that impurities from the reactor etc. are introduced. Low temperature also tends to prevent large deviations in stoichiometry. The element selenium or tellurium can be thought of as being "distilled" in situ, since non-volatile impurities tend to remain in the liquid Se or Te and volatile ones to be swept away by the carrier gas.

2) The other advantages of fabrication are low technological requirements like low temperature, no high power supply, high vacuum or expensive equipments.

3) It automatically provides a good ohmic contact with the semiconductor since the II-VI layer (a few μm thick) is grown directly from the metal plate (1 mm thick) which simultaneously acts as the substrate.

4) The CdSe layers appear to be composed of columnar grains extending from the substrate up to the surface, therefore reducing the presence of grain boundaries in the direction of charge carrier migration, and grain boundaries play a significant role in determine the series resistance of cells and present an obstacle to the attainment of high short-circuit photocurrents.

5) It produces polycrystalline II-VI layers with improved light-harvesting capability. The ratio of actual surface area to geometrical area of these samples is estimated to be about 5. These layers are characterized by a highly absorbing dark surface which makes of them appropriate candidates for applications such as high photovoltaic effects for which single crystallinity is not a prerequisite.

These five advantages result from the fact that, in the liquid metal-vapour reaction, the II-VI semiconducting layer is actually grown from the metal substrate. In this process the metal substrate provides one of the elements necessary to from the semiconductor. This differs markedly from other well known techniques such as vacuum sublimation, electrodeposition, chemical bath deposition, screen-printing, spray pyrolysis and metal-organic chemical vapour deposition, where the II-VI compounds are deposited or grown onto a substrate made of some other material which provides a solid support and electrical contact. The establishment of good ohmic contacts in these cases can be problematic.[39]

These layers do not require extensive post-etching treatments because after growth they already possess a texture surface formed by an agglomeration of pyramid like crystallites.

5.2 Suggestions

For future studies,

1) The doping density of CdTe should be reduced in order to improve photo-current density.

2) In view of the fact that CdTe is not photoelectrochemically stable in aqueous solutions, a nonaqueous electrolyte comprising methanol, tetrabutyl ammonium perchlorate as the supporting electrolyte and ferrocene / ferrocenium ion as the redox species, could be adopted for their photoelectrochemical characterization.[40]

3) Both Se and Te atoms can be made to react with the Cd plate at the same time to produce the ternary compound $CdSe_xTe_{1-x}$. This compound would have a bandgap energy in between the CdSe and CdTe bandgap and possess an increased stability in polysulfide solution, particularly at high values of x. The relative stability of these electrodes was found to be related to their crystal structures. CdTe is normally cubic, while the usual structure of CdSe is hexagonal (see chapter 3). Increase in cubic phase content, paralleling the decrease in the Se atom fraction, leads to a decrease in stability.[41]

4) The addition of cesium cations in sodium polysulfide solution will increase the photocurrent density. Rubin et al.[42] indicate that if all the Na^+ or K^+ are removed by ion exchange so that only Cs^+ is present, the current-potential properties then revert to the "Na^+ or K^+ only" case. Although stability has not been obtained for time periods necessary to consider a practical solar energy converter, the increased stability is a major, promising effect. Stabilization is not observed in the presence of supporting electrolyte containing only Cs^+ or any other alkali cation, stabilization is only obtained in the presence of a Cs^+ / Na^+ or K^+ supporting electrolyte mixture.

Finally eventhough electrochemical techniques are quite useful in providing a quick and reliable way to determine the semiconducting properties and photovoltaic performance of a II-VI compound in electrode form, the lack of long term stability

associated with these electrochemical photovoltaic devices tends to suggest that the solid-state approach using cells of the Schottky barrier type or the heterojunction type may be better suited to practical applications in photovoltaic solar energy conversion.

REFERENCES

1. D. M. Chapin, C. S. Fuller and G. L. Pearson, J. Appl. Phys., 25, 676 (1954)

2. W. H. Brattain and C. G. B. Garrett, Bell System Tech. J., 34, 125 (1955)

3. W. H. Brattain and P. J. Boddy, J. Electrochem. Soc., 109, 574 (1962)

4. A. J. Nozik, Ann. Rev. Phys. Chem., 29, 189 (1978)

5. M. Prince, J. Appl. Phys., 26, 534 (1955)

6. R. O. Loutfy, T. F. McIntyre, D. K. Murti and C. K. Hsiao, Solar Energy Mater., 5, 221 (1981)

7. J. S. Lee, Y. K. Jun and H. B. Im, J. Electrochem. Soc., 134, 249 (1987)

8. R. Haak, D. Tench and M. Russak, J. Electro. Soc., 131, 2709 (1984)

9. M. Tomkiewicz, I. Ling and W. S. Parsons, J. Electrochem. Soc., 129, 2017 (1982)

10. H. O. Finklea, "Semiconductor Electrodes", (1988)

11. D. Iwanov, and C. Nanev, Acta Physica Academiae Scientiarum Hungaricae, 47, 83 (1979)

12. J. S. Curran, R. Philippe, M. Roubin and L. Mosoni, Solar Energy Mater., 9, 329 (1983)

13. M. F. Lawrence, N. Du, R. Philippe and J. P. Dodelet, J. Cryst. Growth, 84, 133 (1987)

14. M. F. Lawrence, N. Du, G. Stremsdoerfer, R. Philippe and J. P. Dodelet, Electrochem. Soc. Ext. Abs., 86-1, 467 (1986)

15. M. F. Lawrence, Z. Deng and L. Gastonguay, Mat. Res. Soc. Symp. Proc., 131, 149 (1989)

16. J. Nishizana, U.S. Patent, 4783426, Nov. 8, 1988

17. J. S. Curran, P. Philippe and G. Stermsdoerfer, J. Electroanal. Chem., 187, 121 (1985)

18. N. Kh. Abrikosov, V. F. Bankina, L. V. Poretskaya, L. E. Shelimova and E. V. Skudnova, "Semiconducting II-VI, IV-VI, and V-VI Compounds", (New York, 1969)

19. S. Chandra, "Photoelectrochemical Solar Cells", (New York 1985)

20. M. A. Russak, J. Reichman, H. Witzke, S. K. Deb and S. N. Chen, J. Electrochem. Soc., 127, 725 (1980)

21. B. Parkinson, J. Chem. Educ., 60, 338 (1983)

22. S. M. Boudreau, R.D. Rauh, and R. A. Boudreau, J. Chem. Educ. 60, 498 (1983)

23. B. G. Streetman, "Solid State Electronic Devices", (New Jersey, 1980)

24. K. Colbow, D. J. Harrison, and B. L. Funt, J. Electrochem. Soc., 128, 547 (1981)

25. P. C. Searson and R. M. Latanision, J. Electrochem. Soc., 135 1358 (1988)

26. M. A. Butler, J. Appl. Phys., 48, 1914 (1977)

27. A. Heller, G. P. Schwartz, R. G. Vadimsky, S. Menezes and B. Miller, J. Electrochem. Soc., 125 1156 (1978)

28. A. B. Ellis, S. W. Kaiser, J. M. Bolts, and M. S. Wrighton, J. Am. Chem. Soc., 99, 2839 (1977)

29. A. J. Bard, J. Phys. Chem., 86, 172 (1982)

30. G. Hodes, Energy Resources through Photochemistry and Catalysis (ed. M. Grazel) 425 (Academic, New York, 1983)

31. G. Hodes, S. J. Fonash, A. Heller, and B. Miller, "Advances in Electrochemistry and Electrochemical Engineering", 13 (ed. H. Gerischer) 113 (Wiley, New York, 1985)

32. W. Giggenbach, Inorg. Chem., 13, 1724 (1974)

33. S. Licht, G. Hodes, and J. Manassen, J. Inorg. Chem., 25, 2486 (1986)

34. S. Licht and J. Manassen, J. Electrochem. Soc., 132, 1076 (1985)

35. S. Licht, Nature, 330, 148 (1987)

36. S. Licht, R. Tenne, G. Dagan, G. Hodes, J. Manassen, and D. Cahen, Appl. Phys. Lett., 46 (6), 608 (1985)

37. S. Licht, R. Tenne, H. Flaisher, and J. Manassen, J. Electrochem. Soc., 133, 52 (1986)

38. S. Licht, J. Phys. Chem., 90, 1096 (1986)

39. L. C. Isett, J. Appl. Phys., 55 3190 (1984)

40. R. N. Bhattacharya and K. Rajeshwar, J. Electrochem. Soc., 131 2032 (1984)

41. G. Hodes, J. Manassen and D. Cahen, J. A. C. S., 102, 5964 (1980)

42. H. D. Rubin, D. J. Arent, B. D. Humphrey, and A. B. Bocarsly, J. Electrochem. Soc., 134 93 (1987)